bioRxiv preprint doi: https://doi.org/10.1101/154963; this version posted June 24, 2017. The copyright holder for this preprint (which was not certified by peer review) is the author/funder. All rights reserved. No reuse allowed without permission.

A new genus of horse from Pleistocene North America

Peter D. Heintzman[a,b*], Grant D. Zazula[c], Ross D.E. MacPhee[d], Eric Scott[e], James A. Cahill[a], Brianna K. McHorse[f], Joshua D. Kapp[a], Mathias Stiller[a,g], Matthew J. Wooller[h,i], Ludovic Orlando[j,k], John R. Southon[l], Duane G. Froese[m], Beth Shapiro[a,n*]

[a] Department of Ecology and Evolutionary Biology, University of California Santa Cruz, Santa Cruz, CA 95064

[b] Tromsø University Museum, UiT - The Arctic University of Norway, 9037 Tromsø, Norway

[c] Yukon Palaeontology Program, Government of Yukon, Whitehorse, YT Y1A 2C6, Canada

[d] Department of Mammalogy, Division of Vertebrate Zoology, American Museum of Natural History, New York, NY 10024

[e] Dr. John D. Cooper Archaeological and Palaeontological Center, California State University Fullerton, Fullerton, CA 92831

[f] Department of Organismal and Evolutionary Biology, Harvard University, Cambridge, MA

[g] Department of Translational Skin Cancer Research, German Consortium for Translational Cancer Research, D-45141 Essen, Germany

[h] College of Fisheries and Ocean Sciences, University of Alaska Fairbanks, 905 N. Koyukuk Dr., Fairbanks AK 99775 USA

[i] Alaska Stable Isotope Facility, Water and Environmental Research Center, University of Alaska Fairbanks, 306 Tanana Loop, Fairbanks AK 99775 USA

[j] Centre for GeoGenetics, Natural History Museum of Denmark, Øster Voldgad 5-7, 1350K Copenhagen, Denmark

bioRxiv preprint doi: https://doi.org/10.1101/154963; this version posted June 24, 2017. The copyright holder for this preprint (which was not certified by peer review) is the author/funder. All rights reserved. No reuse allowed without permission.

[k] Université de Toulouse, Université Paul Sabatier (UPS), Laboratoire AMIS, CNRS UMR 5288, Toulouse, France

[l] Keck-CCAMS Group, Earth System Science Department, University of California, Irvine, CA 92697

[m] Department of Earth and Atmospheric Sciences, University of Alberta, Edmonton, AB T6G 2E3, Canada

[n] UCSC Genomics Institute, University of California Santa Cruz, Santa Cruz, CA 95064

***Corresponding authors**: Peter D. Heintzman: peteheintzman@gmail.com; Beth Shapiro: bashapir@ucsc.edu

bioRxiv preprint doi: https://doi.org/10.1101/154963; this version posted June 24, 2017. The copyright holder for this preprint (which was not certified by peer review) is the author/funder. All rights reserved. No reuse allowed without permission.

Abstract

The extinct "New World stilt-legged", or NWSL, equids constitute a perplexing group of Pleistocene horses endemic to North America. Their slender distal limb bones resemble those of Asiatic asses, such as the Persian onager. Previous palaeogenetic studies, however, have suggested a closer relationship to caballine horses than to Asiatic asses. Here, we report complete mitochondrial and partial nuclear genomes from NWSL equids from across their geographic range. Although multiple NWSL equid species have been named, our palaeogenomic and morphometric analyses support the idea that there was only a single species of middle to late Pleistocene NWSL equid, and demonstrate that it falls outside of crown group *Equus*. We therefore propose a new genus, *Haringtonhippus*, for the sole species *H. francisci*. Our combined genomic and phenomic approach to resolving the systematics of extinct megafauna will allow for an improved understanding of the full extent of the terminal Pleistocene extinction event.

bioRxiv preprint doi: https://doi.org/10.1101/154963; this version posted June 24, 2017. The copyright holder for this preprint (which was not certified by peer review) is the author/funder. All rights reserved. No reuse allowed without permission.

Introduction

The family that includes modern horses, asses, and zebras, the Equidae, is a classic model of macroevolution. The excellent fossil record of this family clearly documents its ~55 million year evolution from dog-sized hyracotheres through many intermediate forms and extinct offshoots to present-day *Equus*, which comprises all living equid species (MacFadden, 1992). The downside of this excellent fossil record is that many dubious fossil equid taxa have been erected, a problem especially acute within Pleistocene *Equus* of North America (Macdonald & Toohey, 1992). While numerous species are described from the fossil record, molecular data suggest that most belonged to, or were closely related to, a single, highly variable stout-legged caballine species that includes the domestic horse, *E. caballus* (Weinstock *et al*., 2005). The enigmatic and extinct "New World stilt-legged" (NWSL) forms, however, exhibit a perplexing mix of morphological characters, including slender, stilt-like distal limb bones with narrow hooves reminiscent of extant Eurasian hemionines, the Asiatic wild asses (*E. hemionus*, *E. kiang*) (Eisenmann, 1992; Eisenmann *et al*., 2008; Harington & Clulow, 1973; Lundelius & Stevens, 1970; Scott, 2004), and dentitions that have been interpreted as more consistent with either caballine horses (Lundelius & Stevens, 1970) or hemionines (MacFadden, 1992).

On the basis of their slender distal limb bones, the NWSL equids have traditionally been considered as allied to hemionines (e.g. (Eisenmann *et al*., 2008; Guthrie, 2003; Scott, 2004; Skinner & Hibbard, 1972)). Palaeogenetic analyses based on mitochondrial DNA (mtDNA) have, however, consistently placed NWSL equids closer to caballine horses (Der Sarkissian *et al*., 2015; Orlando *et al*., 2008, 2009; Vilstrup *et al*., 2013; Weinstock *et al*., 2005). The current mtDNA-based phylogenetic model therefore suggests that the stilt-legged morphology arose independently in the New and Old Worlds (Weinstock *et al*., 2005), and may represent

bioRxiv preprint doi: https://doi.org/10.1101/154963; this version posted June 24, 2017. The copyright holder for this preprint (which was not certified by peer review) is the author/funder. All rights reserved. No reuse allowed without permission.

convergent adaptations to arid climates and habitats (Eisenmann, 1985). However, these models have been based on two questionable sources. The first is based on 4 short control region sequences (<1000 base pairs, bp; (Weinstock *et al*., 2005)), a data type that can be unreliable for resolving the placement of major equid groups (Der Sarkissian *et al*., 2015; Orlando *et al*., 2009). The second consist of 2 mitochondrial genome sequences (Vilstrup *et al*., 2013) that are either incomplete or otherwise problematic (see Results). Given continuing uncertainty regarding the phylogenetic placement of NWSL equids—which impedes our understanding of Pleistocene equid evolution in general—we therefore sought to resolve their position using multiple mitochondrial and partial nuclear genomes from specimens representing as many parts of late Pleistocene North America as possible.

The earliest recognized NWSL equid fossils date to the late Pliocene/early Pleistocene (~2-3 million years ago, Ma) of New Mexico (Azzaroli & Voorhies, 1993; Eisenmann, 2003; Eisenmann *et al*., 2008)). Middle and late Pleistocene forms tended to be smaller in stature than their early Pleistocene kin, and ranged across southern and extreme northwestern North America (i.e., eastern Beringia, which includes Alaska, USA and Yukon Territory, Canada). NWSL equids have been assigned to several named species, such as *E. tau* Owen 1869, *E. francisci* Hay 1915, *E. calobatus* Troxell 1915, and *E. (Asinus)* cf. *kiang*, but there is considerable confusion and disagreement regarding their taxonomy. Consequently, some researchers have chosen to refer to them collectively as *Equus* (*Hemionus*) spp. (Guthrie, 2003; Scott, 2004), or avoid a formal taxonomic designation altogether (Der Sarkissian *et al*., 2015; Vilstrup *et al*., 2013; Weinstock *et al*., 2005). Using our phylogenetic framework and comparisons between specimens identified by palaeogenomics and/or morphology, we attempted to determine the taxonomy of middle-late Pleistocene NWSL equids.

bioRxiv preprint doi: https://doi.org/10.1101/154963; this version posted June 24, 2017. The copyright holder for this preprint (which was not certified by peer review) is the author/funder. All rights reserved. No reuse allowed without permission.

93 Radiocarbon (^{14}C) dates from Gypsum Cave, Nevada, confirm that NWSL equids
94 persisted in areas south of the continental ice sheets during the last glacial maximum (LGM;
95 ~26-19 thousand radiocarbon years before present (ka BP; (Clark *et al*., 2009)) until near the
96 terminal Pleistocene, ~13 thousand radiocarbon years before present (^{14}C ka BP) (Weinstock *et*
97 *al*., 2005), soon after which they became extinct, along with their caballine counterparts and
98 most other coeval species of megafauna (Koch & Barnosky, 2006). This contrasts with dates
99 from unglaciated eastern Beringia, where NWSL equids were seemingly extirpated locally
100 during a relatively mild interstadial interval centered on ~31 ^{14}C ka BP (Guthrie, 2003), thus
101 prior to the LGM (Clark *et al*., 2009), final loss of caballine horses (Guthrie, 2003, 2006), and
102 arrival of humans in the region (Guthrie, 2006). The apparently discrepant extirpation
103 chronology between NWSL equids south and north of the continental ice sheets implies that their
104 populations responded variably to demographic pressures in different parts of their range, which
105 is consistent with results from some other megafauna (Guthrie, 2006; Heintzman *et al*., 2015;
106 Zazula *et al*., 2014). To further test this extinction chronology, we generated new radiocarbon
107 dates from eastern Beringian NWSL equids.
108 We analyzed 26 full mitochondrial genomes and 17 partial nuclear genomes from late
109 Pleistocene NWSL equids, which revealed that individuals from both eastern Beringia and
110 southern North America form a single well-supported clade that falls outside the diversity of
111 *Equus* and diverged from the lineage leading to *Equus* during the latest Miocene or early
112 Pliocene. This novel and robust phylogenetic placement warrants the recognition of NWSL
113 equids as a distinct genus, which we here name *Haringtonhippus*. After reviewing potential
114 species names, and conducting morphometric and anatomical comparisons, we determined that
115 *francisci* Hay is the most well-supported species name, and we therefore refer the analyzed

bioRxiv preprint doi: https://doi.org/10.1101/154963; this version posted June 24, 2017. The copyright holder for this preprint (which was not certified by peer review) is the author/funder. All rights reserved. No reuse allowed without permission.

116 NWSL equid specimens to *H. francisci*. New radiocarbon dates revealed that *H. francisci* was
117 extirpated in eastern Beringia ~14 ^{14}C ka BP. In light of our analyses, we review the Plio-
118 Pleistocene evolutionary history of equids, and the implications for the systematics of equids and
119 other Pleistocene megafauna.
120

bioRxiv preprint doi: https://doi.org/10.1101/154963; this version posted June 24, 2017. The copyright holder for this preprint (which was not certified by peer review) is the author/funder. All rights reserved. No reuse allowed without permission.

Results

Phylogeny of North American late Pleistocene and extant equids

We reconstructed whole mitochondrial genomes from 26 NWSL equids and four New World caballine *Equus* (two *E. lambei*, two *E.* cf. *scotti*). Using these and mitochondrial genomes of representatives from all extant and several late Pleistocene equids, we estimated a mitochondrial phylogeny, using a variety of outgroups (Appendix 1, Supplementary tables 1-2 and Supplementary file 1). The resulting phylogeny is mostly consistent with previous studies (Der Sarkissian *et al*., 2015; Vilstrup *et al*., 2013), including confirmation of NWSL equid monophyly (Weinstock *et al*., 2005). However, we recover a strongly supported placement of the NWSL equid clade outside of crown group diversity (*Equus*), but closer to *Equus* than to *Hippidion* (Figure 1 and Appendix 2, Figure 1-Figure supplement 1a and Supplementary tables 1-3). In contrast, previous palaeogenetic studies placed the NWSL equids within crown group *Equus*, closer to caballine horses than to non-caballine asses and zebras (Der Sarkissian *et al*., 2015; Orlando *et al*., 2008, 2009; Vilstrup *et al*., 2013; Weinstock *et al*., 2005). To explore possible causes for this discrepancy, we reconstructed mitochondrial genomes from previously sequenced NWSL equid specimens and used a maximum likelihood evolutionary placement algorithm (Berger *et al*., 2011) to place these published sequences in our phylogeny *a posteriori*. These analyses suggested that previous results were likely due to a combination of outgroup choice and the use of short, incomplete, or problematic mtDNA sequences (Appendix 2 and Supplementary table 4).

To confirm the mtDNA result that NWSL equids fall outside of crown group equid diversity, we sequenced and compared partial nuclear genomes from 17 NWSL equids to a caballine (horse) and a non-caballine (donkey) reference genome. After controlling for reference

bioRxiv preprint doi: https://doi.org/10.1101/154963; this version posted June 24, 2017. The copyright holder for this preprint (which was not certified by peer review) is the author/funder. All rights reserved. No reuse allowed without permission.

144 genome and ancient DNA fragment length artifacts (Appendices 1-2), we examined differences
145 in relative private transversion frequency between these genomes (Appendix 1-figure 1). We
146 found that the relative private transversion frequency for NWSL equids was ~1.4-1.5 times
147 greater than that for horse or donkey (Appendix 2, Supplementary table 5, Figure 1-Figure
148 supplement 2, and Supplementary file 2). This result supports the placement of NWSL equids as
149 sister to the horse-donkey clade (Figure 1-Figure supplement 3), the latter of which is
150 representative of living *Equus* diversity (e.g. (Der Sarkissian *et al*., 2015; Jónsson *et al*., 2014)),
151 and is therefore congruent with the mitochondrial genomic analyses.
152

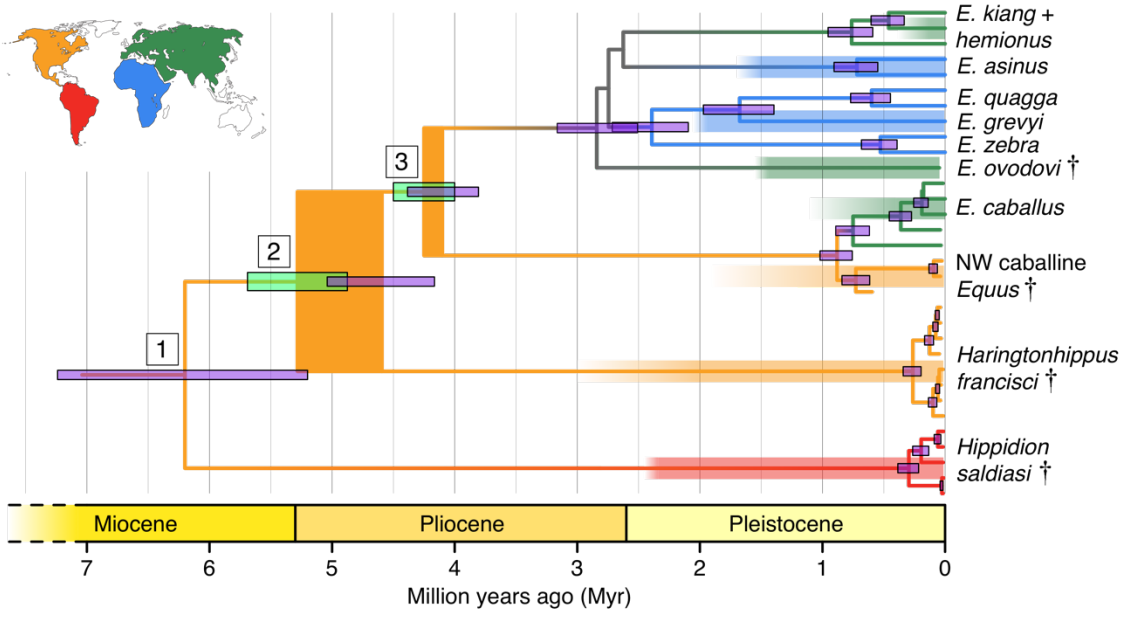

153

154 **Figure 1.** Phylogeny of extant and middle-late Pleistocene equids, as inferred from the Bayesian
155 analysis of full mitochondrial genomes. Purple node bars illustrate the 95% highest posterior
156 density of node heights and are shown for nodes with >0.99 posterior probability support. The
157 range of divergence estimates derived from the analysis of nuclear genomes is shown by the
158 thicker lime green node bars ((Orlando *et al*., 2013); this study). Major nodes are labelled with

bioRxiv preprint doi: https://doi.org/10.1101/154963; this version posted June 24, 2017. The copyright holder for this preprint (which was not certified by peer review) is the author/funder. All rights reserved. No reuse allowed without permission.

159 boxed numbers. The thicknesses of nodes 2 and 3 represent the range between the median
160 nuclear and mitochondrial genomic divergence estimates. Branches are coloured based on
161 species provenance and the most parsimonious biogeographic scenario given the data, with gray
162 indicating ambiguity. Fossil record occurrences for major represented groups (including South
163 American *Hippidion*, New World stilt-legged equids, and Old World Sussemiones) are
164 represented by the geographically-coloured bars, with fade indicating uncertainty in the first
165 appearance datum (after (Eisenmann *et al*., 2008; Forsten, 1992; O'Dea *et al*., 2016; Orlando *et*
166 *al*., 2013) and references therein). The Asiatic ass species (*E. kiang*, *E. hemionus*) are not
167 reciprocally monophyletic based on the analyzed mitochondrial genomes, and so the Asiatic ass
168 clade is shown as '*E. kiang* + *hemionus*'. Daggers denote extinct taxa. NW: New World.
169

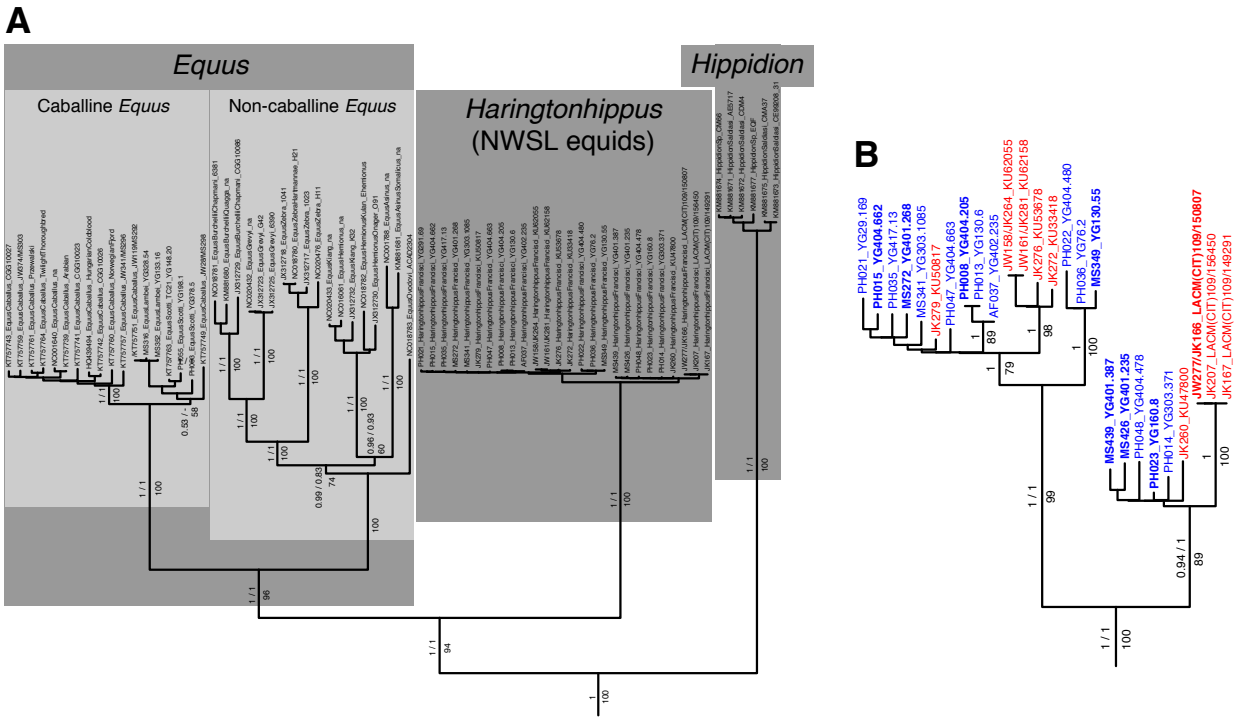

170

171 **Figure 1-Figure supplement 1.** An example maximum likelihood (ML) phylogeny of equid
172 mitochondrial genomes. This topology resulted from the analysis of mtDNA data set 3 (see

bioRxiv preprint doi: https://doi.org/10.1101/154963; this version posted June 24, 2017. The copyright holder for this preprint (which was not certified by peer review) is the author/funder. All rights reserved. No reuse allowed without permission.

Appendix 1) with all partitions and *Hippidion* included, and dog and ceratomorphs as outgroup (not shown). Numbers above branches are Bayesian posterior probability support values from equivalent MrBayes and BEAST analyses, with those below indicating ML bootstrap values calculated in RAxML, and are shown for major nodes. (A) Full phylogeny of the analyzed equid sequences. (B) The *Haringtonhippus* (NWSL equid) clade, with tips color coded by geographic origin: Beringia, blue; contiguous USA, red. Tips in bold were included in the BEAST analysis (see also Supplementary file 1).

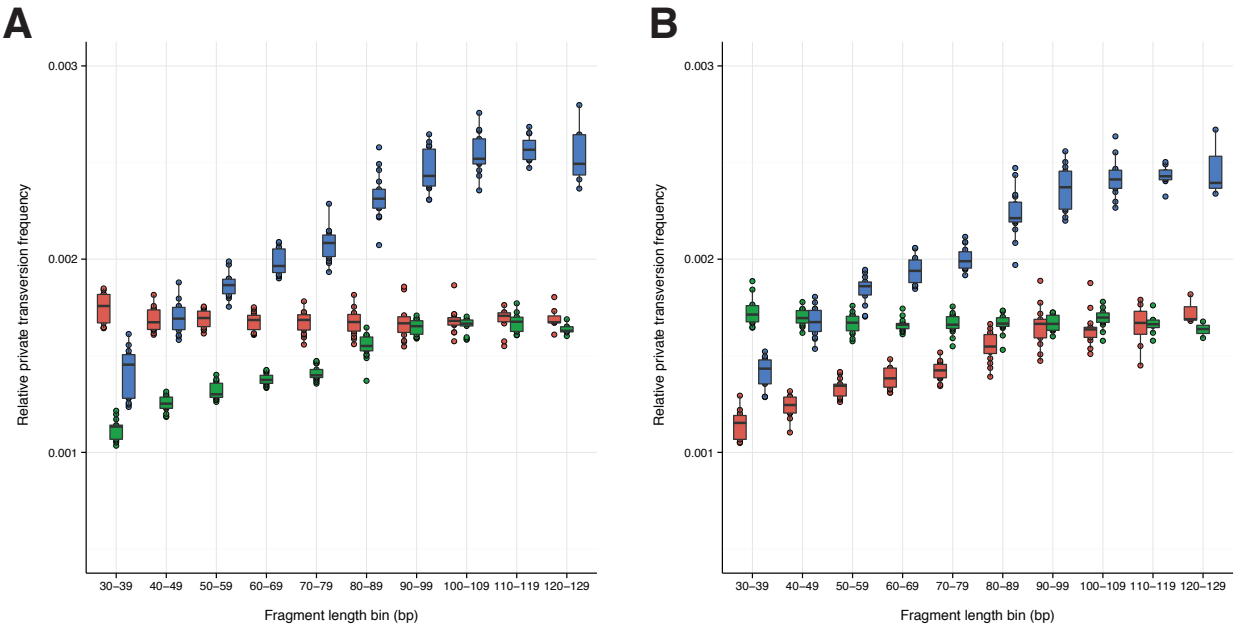

Figure 1-Figure supplement 2. A comparison of relative private transversion frequencies between the nuclear genomes of a caballine *Equus* (horse, *E. caballus*; green), a non-caballine *Equus* (donkey, *E. asinus*; red), and 17 NWSL equids (=*Haringtonhippus francisci*; blue) at different read lengths, with reads divided into 10 base pair (bp) bins. Analyses are based on alignment to the horse (A) or donkey (B) genome coordinates. To account for bins with low data content, we only display comparisons with at least 200,000 observable sites.

bioRxiv preprint doi: https://doi.org/10.1101/154963; this version posted June 24, 2017. The copyright holder for this preprint (which was not certified by peer review) is the author/funder. All rights reserved. No reuse allowed without permission.

188

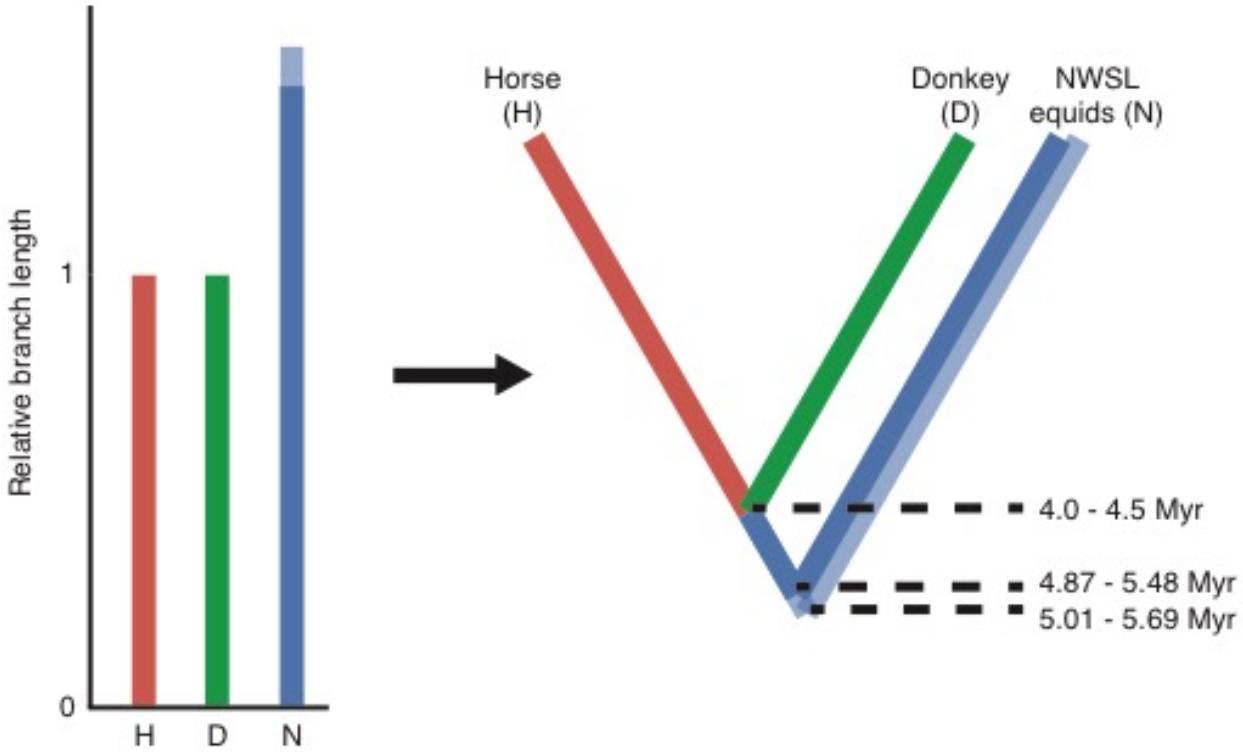

189

190 **Figure 1-Figure supplement 3.** Calculation of divergence date estimates from nuclear genome
191 data. Relative branch lengths are from Supplementary table 5. Minimum (darker blue) and
192 maximum (lighter blue) estimates are shown for the NWSL equid branch.

193

194 **Divergence times of *Hippidion*, NWSL equids, and *Equus***

195 We estimated the divergence times between the lineages leading to *Hippidion*, the NWSL
196 equids, and *Equus*. We first applied a Bayesian time-tree approach to the whole mitochondrial
197 genome data. This gave divergence estimates for the *Hippidion*-NWSL/*Equus* split (node 1) at
198 5.15-7.66 Ma, consistent with (Der Sarkissian *et al*., 2015), the NWSL-*Equus* split (node 2) at
199 4.09-5.13 Ma, and the caballine/non-caballine *Equus* split (node 3) at 3.77-4.40 Ma (Figure 1
200 and Supplementary table 3). These estimates suggest that the NWSL-*Equus* mitochondrial split

bioRxiv preprint doi: https://doi.org/10.1101/154963; this version posted June 24, 2017. The copyright holder for this preprint (which was not certified by peer review) is the author/funder. All rights reserved. No reuse allowed without permission.

occurred only ~500 thousand years (ka) prior to the caballine/non-caballine *Equus* split. We then estimated the NWSL-*Equus* divergence time using relative private transversion frequency ratios between the nuclear genomes, assuming a caballine/non-caballine *Equus* divergence estimate of 4-4.5 Ma (Orlando *et al*., 2013) and a genome-wide strict molecular clock (following (Heintzman *et al*., 2015)). This analysis yielded a divergence estimate of 4.87-5.69 Ma (Figure 1-Figure supplement 3), which overlaps with that obtained from the relaxed clock analysis of whole mitochondrial genome data (Figure 1). These analyses suggest that the NWSL equid and *Equus* clades diverged during the latest Miocene or early Pliocene (4.1-5.7 Ma; late Hemphillian or earliest Blancan).

Systematic Palaeontology

Previous palaeontological and palaeogenetic studies have uniformly placed NWSL equids within genus *Equus* (Der Sarkissian *et al*., 2015; Harington & Clulow, 1973; Orlando et al., 2008, 2009; Scott, 2004; Vilstrup *et al*., 2013; Weinstock *et al*., 2005). This, however, conflicts with the phylogenetic signal provided by palaeogenomic data, which strongly suggest that NWSL equids fall outside the confines of this genus. Nor is there any morphological or genetic evidence warranting the assignment of NWSL equids to an existing extinct taxon such as *Hippidion*. We therefore erect a new genus for NWSL equids, *Haringtonhippus*, as defined and delimited below:

Order: Perissodactyla, Owen 1848

Family: Equidae, Linnaeus 1758

Subfamily: Equinae, Steinmann & Döderlein 1890

Tribe: Equini, Gray 1821

bioRxiv preprint doi: https://doi.org/10.1101/154963; this version posted June 24, 2017. The copyright holder for this preprint (which was not certified by peer review) is the author/funder. All rights reserved. No reuse allowed without permission.

224 Genus: *Haringtonhippus*, gen. nov.

225

226 *Type species*. *Haringtonhippus francisci* Hay 1915.

227

228 *Etymology.* The new genus is named in honor of C. Richard Harington, who first described
229 NWSL equids from eastern Beringia (Harington & Clulow, 1973). '*Hippus*' is from the Greek
230 word for horse, and so *Haringtonhippus* is implied to mean 'Harington's horse'.

231

232 *Holotype*. A partial skeleton consisting of a complete cranium, mandible, and a stilt-legged third
233 metatarsal (MTIII) (Figure 2a and Figure 2-Figure supplement 1b), which is curated at the
234 University of Texas, Austin (Texas Memorial Museum (TMM) 34-2518). This specimen is the
235 holotype of '*E*'. *francisci*, originally described by Hay (1915), and is from the middle
236 Pleistocene Lissie Formation of Wharton County, Texas (Hay, 1915; Lundelius & Stevens,
237 1970).).

238

bioRxiv preprint doi: https://doi.org/10.1101/154963; this version posted June 24, 2017. The copyright holder for this preprint (which was not certified by peer review) is the author/funder. All rights reserved. No reuse allowed without permission.

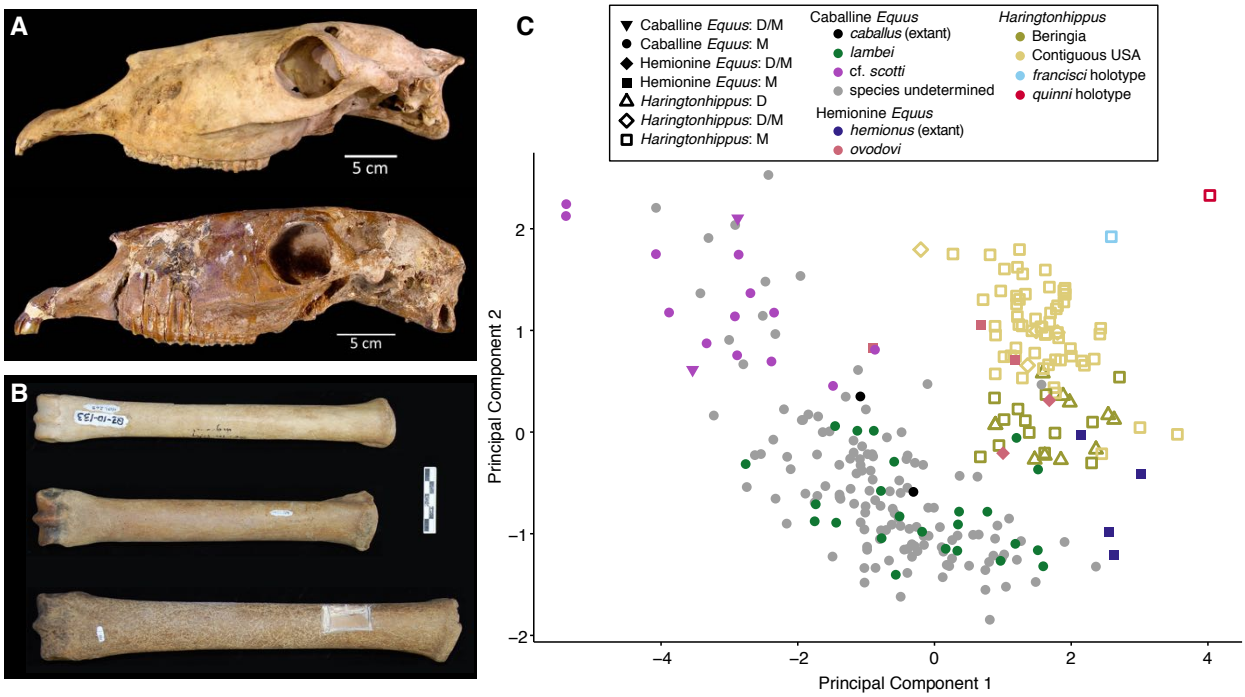

239

240 **Figure 2.** Morphological analysis of extant and middle-late Pleistocene equids. (A) Crania of

241 *Haringtonhippus francisci*, upper: LACM(CIT) 109/156450 from Nevada, lower: TMM 34-2518

242 from Texas. (B) From upper to lower, third metatarsals of: *H. francisci* (YG 401.268), *E. lambei*

243 (YG 421.84), and *E.* cf. *scotti* (YG 198.1) from Yukon. Scale bar is 5 cm. (C) Principal

244 component analysis of selected third metatarsals from extant and middle-late Pleistocene equids,

245 showing clear clustering of stilt-legged (hemionine(-like) *Equus* and *H. francisci*) from stout-

246 legged (caballine *Equus*) specimens (see also Supplementary file 4). The first and second

247 principal components explain 95% of the variance. Specimen identifications were derived from

248 DNA (D) and/or morphology (M).

249

bioRxiv preprint doi: https://doi.org/10.1101/154963; this version posted June 24, 2017. The copyright holder for this preprint (which was not certified by peer review) is the author/funder. All rights reserved. No reuse allowed without permission.

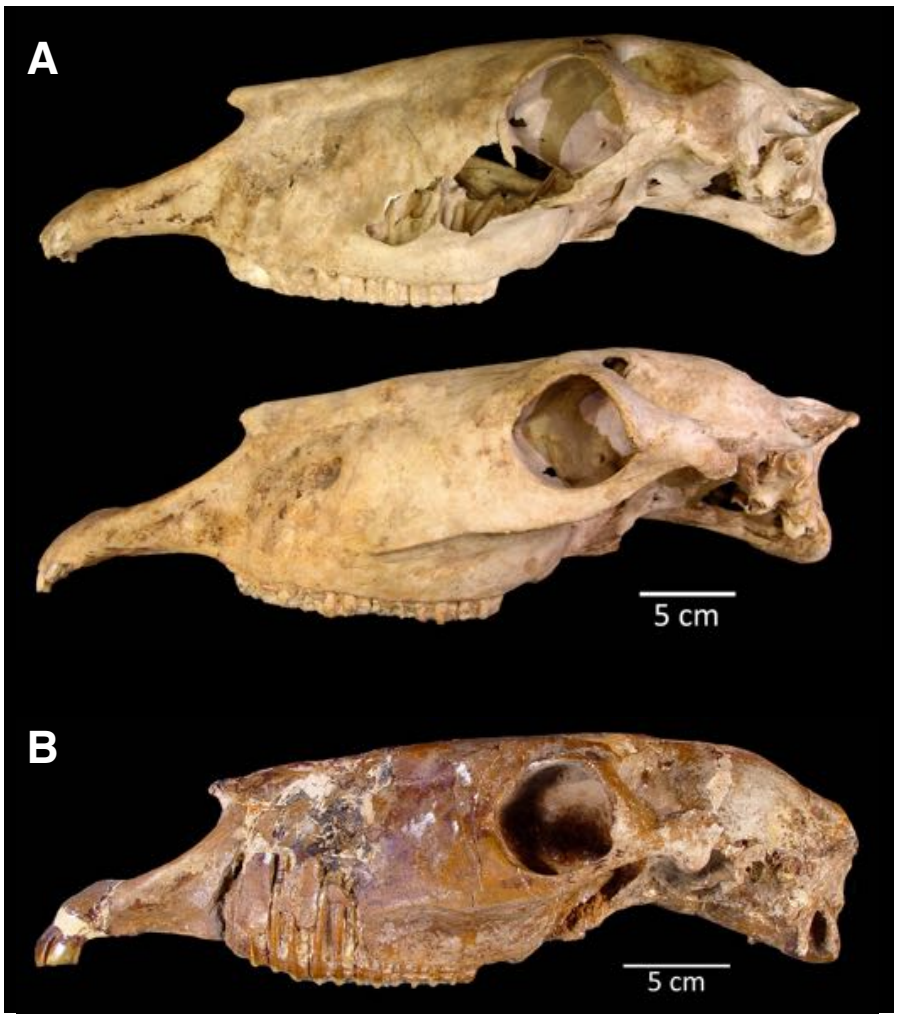

Figure 2-Figure supplement 1. The two crania assigned to *H. francisci*. (A) LACM(CIT) 109/156450 from Nevada, identified through mitochondrial and nuclear palaeogenomic analysis. Upper: right side (reflected for comparison), lower: left side. (B) Part of the *H. francisci* holotype, TMM 34-2518 from Texas.

bioRxiv preprint doi: https://doi.org/10.1101/154963; this version posted June 24, 2017. The copyright holder for this preprint (which was not certified by peer review) is the author/funder. All rights reserved. No reuse allowed without permission.

Figure 2-Figure supplement 2. Comparison between the limb bones of *H. francisci*, *E. lambei*, and *E.* cf. *scotti* from Yukon. (A) Third metatarsals from *H. francisci* (upper; YG 401.268), *E. lambei* (middle; YG 421.84), and *E.* cf. *scotti* (lower; YG 198.1). (B) Third metacarpals from *H. francisci* (upper; YG 404.663), *E. lambei* (middle; YG 109.6), and *E.* cf. *scotti* (lower; YG 378.15). (C) Proximal fragments of radii from *H. francisci* (left; YG 303.1085), and *E. lambei* (right; YG 303.325). (D) First phalanges from *H. francisci* (left; YG 130.3), *E. lambei* (middle; YG 404.22), and *E.* cf. *scotti* (right; YG 168.1).

bioRxiv preprint doi: https://doi.org/10.1101/154963; this version posted June 24, 2017. The copyright holder for this preprint (which was not certified by peer review) is the author/funder. All rights reserved. No reuse allowed without permission.

Figure 2-Figure supplement 3. An example equid metacarpal from Natural Trap Cave, Wyoming (KU 47800; JK260), originally referred to *Equus* sp., but here identified as *H. francisci* on the basis of mitochondrial and nuclear genome data. We note the relative slenderness of this specimen, which is comparable to YG 404.663 (*H. francisci*) from Yukon in Figure 2-Figure supplement 2.

Figure 2-Figure supplement 4. An example femur of *H. francisci* from Gypsum Cave, Nevada (LACM(CIT)109/150708; JW277 / JK166), originally identified by Weinstock and colleagues (2005).

bioRxiv preprint doi: https://doi.org/10.1101/154963; this version posted June 24, 2017. The copyright holder for this preprint (which was not certified by peer review) is the author/funder. All rights reserved. No reuse allowed without permission.

278 *Referred material.* On the basis of mitochondrial and nuclear genomic data, we assign the
279 following material to *Haringtonhippus*: a cranium, femur, and MTIII (LACM(CIT); Nevada);
280 three MTIIIs and three third metacarpals (MCIII) (KU; Wyoming); two radii, 12 MTIII, three
281 MCIII, a metapodial, and a first phalanx (YG; Yukon Territory) (Figure 2-Figure supplements 1-
282 4 and Supplementary file 1; (Weinstock *et al*., 2005)). This material includes 5 males and at least
283 6 females (Appendix 2, Supplementary table 6 and Supplementary file 3). We further assign
284 MTIII specimens from Yukon Territory (n=13), Wyoming (n=57), and Nevada (n=4) to
285 *Haringtonhippus* on the basis of morphometric analysis (Figure 2c and Supplementary file 4).
286 We tentatively assign 19 NWSL equid metapodial specimens from Alaska (Guthrie, 2003) to
287 *Haringtonhippus*, but note that morphometric and/or palaeogenomic analysis would be required
288 to confirm this designation.
289
290 *Geographic and temporal distribution*. *Haringtonhippus* is known only from the Pleistocene of
291 North America (Figure 1). In addition to the middle Pleistocene holotype from Texas,
292 *Haringtonhippus* is confidently known from the late Pleistocene of Yukon Territory (Klondike),
293 Wyoming (Natural Trap Cave), and Nevada (Gypsum Cave, Mineral Hill Cave), and is
294 tentatively registered as present in Alaska (Appendix 2, Supplementary file 1, and
295 Supplementary table 4; (Vilstrup *et al*., 2013; Weinstock *et al*., 2005)).
296 To investigate the last appearance date (LAD) of *Haringtonhippus* in eastern Beringia,
297 we obtained new radiocarbon dates from 17 Yukon Territory fossils (Appendix 1 and
298 Supplementary file 1). This resulted in three statistically-indistinguishable radiocarbon dates of
299 ~14.4 ^{14}C ka BP (derived from two independent laboratories) from a metacarpal bone (YG
300 401.235) of *Haringtonhippus*, which represents this taxon's LAD in eastern Beringia

bioRxiv preprint doi: https://doi.org/10.1101/154963; this version posted June 24, 2017. The copyright holder for this preprint (which was not certified by peer review) is the author/funder. All rights reserved. No reuse allowed without permission.

(Supplementary file 1). The LAD for North America as a whole is based on two dates of ~13.1 ^{14}C ka BP from Gypsum Cave, Nevada (Supplementary file 1; (Weinstock *et al*., 2005)).

Mitogenomic diagnosis. *Haringtonhippus* is the sister genus to *Equus* (equid crown group), with *Hippidion* being sister to the *Haringtonhippus*-*Equus* clade (Figure 1). *Haringtonhippus* can be differentiated from *Equus* and *Hippidion* by 178 synapomorphic positions in the mitochondrial genome, including four insertions and 174 substitutions (Appendix 2, Supplementary table 7 and Supplementary file 5). We caution that these synapomorphies are tentative and will likely be reduced in number as a greater diversity of mitochondrial genomes for extinct equids become available.

Morphological comparisons of third metatarsals. We used morphometric analysis of caballine/stout-legged *Equus* and stilt-legged equids (hemionine/stilt-legged *Equus*, *Haringtonhippus*) MTIIIs to determine how confidently these groups can be distinguished (Figure 2c). Using logistic regression on principal components, we find a strong separation that can be correctly distinguished with 98.2% accuracy (Appendix 2 and Supplementary file 6). Hemionine/stilt-legged *Equus* MTIIIs occupy the same morphospace as *H. francisci* in our analysis, although given a larger sample size, it may be possible to discriminate *E. hemionus* from the remaining stilt-legged equids. We note that *Haringtonhippus* seems to exhibit a negative correlation between latitude and MTIII length, and that specimens from the same latitude occupy similar morphospace regardless of whether DNA- or morphological-based identification was used (Figure 2c and Supplementary file 4).

bioRxiv preprint doi: https://doi.org/10.1101/154963; this version posted June 24, 2017. The copyright holder for this preprint (which was not certified by peer review) is the author/funder. All rights reserved. No reuse allowed without permission.

Comments. On the basis of morphology, we assign all referred material of *Haringtonhippus* to the single species *H. francisci* Hay 1915 (Appendix 2). Comparison between the cranial anatomical features of LACM(CIT) 109/156450 and TMM 34-2518 reveal some minor differences, which can likely be ascribed to intraspecific variation (Fig 2a and Appendix 2 and Figure 2-Figure supplement 1). Further, the MTIII of TMM 34-2518 is comparable to the MTIIIs ascribed to *Haringtonhippus* by palaeogenomic data, and is consistent with the observed latitudinally-correlated variation in MTIII length across *Haringtonhippus* (Figure 2c and Appendix 2).

This action is supported indirectly by molecular evidence, namely the lack of mitochondrial phylogeographic structure and the estimated time to most recent common ancestor (tMRCA) for sampled *Haringtonhippus*. The mitochondrial tree topology within *Haringtonhippus* does not exhibit phylogeographic structure (Figure 1-Figure supplement 1b), which is consistent with sampled *Haringtonhippus* mitochondrial genomes belonging to the same species. Using Bayesian time-tree analysis, we estimated a tMRCA for the sampled *Haringtonhippus* mitochondrial genomes of ~200-470 ka BP (Figure 1 and Supplementary table 3 and Supplementary file 7). The MRCA of *Haringtonhippus* is therefore more recent than that of other extant equid species (such as *E. asinus* and *E. quagga*, which have a combined 95% HPD range: 410-1030 ka BP; Figure 1 and Supplementary table 3 and Supplementary file 7). Although the middle Pleistocene holotype TMM 34-2518 (~125-780 ka BP) may predate our *Haringtonhippus* mitochondrial tMRCA, this sample has no direct date and the range of possible ages falls within the tMRCA range of other extant equid species. We therefore cannot reject the hypothesis of its conspecificity with *Haringtonhippus,* as defined palaeogenomically. We attempted, but were unable, to recover either collagen or genomic data from TMM 34-2518

bioRxiv preprint doi: https://doi.org/10.1101/154963; this version posted June 24, 2017. The copyright holder for this preprint (which was not certified by peer review) is the author/funder. All rights reserved. No reuse allowed without permission.

347 (Appendix 2), consistent with the taphonomic, stratigraphic, and geographic context of this fossil
348 (Hay, 1915; Lundelius & Stevens, 1970). Altogether, the molecular evidence is consistent with
349 the assignment of *H. francisci* as the type and only species of *Haringtonhippus*.
350

bioRxiv preprint doi: https://doi.org/10.1101/154963; this version posted June 24, 2017. The copyright holder for this preprint (which was not certified by peer review) is the author/funder. All rights reserved. No reuse allowed without permission.

Discussion

Reconciling the genomic and fossil records of Plio-Pleistocene equid evolution

The placement of *Haringtonhippus* as sister taxon to *Equus* is less congruent with the fossil record than previous hypotheses, which have placed *Haringtonhippus* within *Equus*, as sister to either hemionines or caballine horses (Figure 1). The earliest NWSL and caballine equids appear in the fossil record at ~2-3 and ~1.9-0.7 Ma (Eisenmann *et al*., 2008; Forsten, 1992), respectively, whereas our divergence estimates suggest that these lineages appeared at 4.1-5.8 and 3.8-4.5 Ma, most likely in North America. This could be due to incompleteness of the fossil record or a discordance between the timing of species divergence and the evolution of diagnostic anatomical characteristics (Forsten, 1992). Although there will likely always be problems associated with the completeness of the fossil record, the well known late Miocene and Pliocene fossil records of New World equids would suggest that this discordance is not due to missing fossils.

Pliocene *Equus* generally exhibits a primitive ('plesippine' in North America, 'stenonid' in the Old World) morphology that presages living zebras and asses (Forsten, 1988, 1992), with more derived caballine (stout-legged) and hemionine (stilt-legged) forms evolving in the early Pleistocene. The stilt-legged morphology appears to have evolved independently at least once in each of the Old and New Worlds, yielding the Asiatic wild asses and *Haringtonhippus*, respectively. We include the middle-late Pleistocene Eurasian *E. hydruntinus* within the Asiatic wild asses (following (Bennett *et al*., 2017; Burke, Eisenmann, & Ambler, 2003; Orlando *et al*., 2006)), and note that the Old World sussemione *E. ovodovi* may represent another instance of independent stilt-legged origin, but its relation to Asiatic wild asses and other non-caballine *Equus* is currently unresolved (as depicted in (Der Sarkissian *et al*., 2015; Orlando *et al*., 2009;

bioRxiv preprint doi: https://doi.org/10.1101/154963; this version posted June 24, 2017. The copyright holder for this preprint (which was not certified by peer review) is the author/funder. All rights reserved. No reuse allowed without permission.

374 Vilstrup *et al*., 2013) and Figure 1). As such, it is plausible that the more primitive Pleistocene
375 morphological states, including *Hippidion*-like, only survived past the early to middle
376 Pleistocene at lower latitudes (South America, Africa; Figure 1), and that the derived hemionine
377 and caballine morphologies evolved from, and replaced, primitive ancestors in higher latitude
378 North America and Eurasia during the Pleistocene, perhaps as adaptations to the extreme
379 ecological pressures perpetuated by the advance and retreat of continental ice sheets in response
380 to rapid climate oscillations during glacial cycles (Forsten, 1992, 1996). We note that this high
381 latitude replacement model is consistent with the turnover observed in the Pleistocene equid
382 regional fossil records of North America (Azzaroli, 1992; Azzaroli & Voorhies, 1993) and
383 Eurasia (Forsten, 1988, 1992, 1996). By contrast, in South America *Hippidion* co-existed with
384 caballine horses until they both succumbed to extinction with much of the New World
385 megafauna near the end of the Pleistocene (Forsten, 1996; Koch & Barnosky, 2006; O'Dea *et al*.,
386 2016). This model helps explain the discordance between the timings of the appearance of the
387 caballine and hemionine morphologies in the fossil record and the divergence of lineages leading
388 to these forms as estimated from palaeogenomic data. The model predicts that some previously
389 described North American Pliocene and early Pleistocene primitive *Equus* species (e.g., *E.*
390 *simplicidens*, *E. idahoensis*; (Azzaroli & Voorhies, 1993)), or specimens thereof, may be
391 ancestral to extant *Equus* and/or late Pleistocene *Haringtonhippus*.
392
393 **Temporal and geographic range overlap of Pleistocene equids in North America**
394 Three new radiocarbon dates of ~14.4 ^{14}C ka BP from a Yukon *Haringtonhippus* fossil greatly
395 extends the known temporal range of this genus in eastern Beringia. This result demonstrates,
396 contrary to its previous LAD of 31,400±1200 ^{14}C years ago (AA 26780; (Guthrie, 2003)), that

bioRxiv preprint doi: https://doi.org/10.1101/154963; this version posted June 24, 2017. The copyright holder for this preprint (which was not certified by peer review) is the author/funder. All rights reserved. No reuse allowed without permission.

397 *Haringtonhippus* survived throughout the last glacial maximum in eastern Beringia (Clark *et al*.,
398 2009) and may have come into contact with humans near the end of the Pleistocene (Goebel,
399 Waters, & O'Rourke, 2008; Guthrie, 2006). These data suggest that populations of stilt-legged
400 *Haringtonhippus* and stout-legged caballine *Equus* were sympatric, both north and south of the
401 continental ice sheets, through the late Pleistocene and became extinct at roughly the same time.
402 The near synchronous extinction of both horse groups across their entire range in North America
403 suggests that similar causal mechanisms may have led each to their demise.

404 The sympatric nature of these equids raises questions of whether they managed to live
405 within the same community without hybridizing or competing for resources. Extant members of
406 the genus *Equus* vary considerably in the sequence of Prdm9, a gene involved in the speciation
407 process, and chromosome number (karyotype) (Ryder, Epel, & Benirschke, 1978; Steiner &
408 Ryder, 2013), and extant caballine and non-caballine *Equus* rarely produce fertile offspring
409 (Allen & Short, 1997; Steiner & Ryder, 2013). It is unlikely, therefore, that the more deeply
410 diverged *Haringtonhippus* and caballine *Equus* would have been able to hybridize. Future
411 analysis of high coverage nuclear genomes, ideally including an outgroup such as *Hippidion*,
412 will make it possible to test for admixture that may have occurred soon after the lineages leading
413 to *Haringtonhippus* and *Equus* diverged, as occurred between the early caballine and non-
414 caballine *Equus* lineages (Jónsson et al., 2014). It may also be possible to use isotopic and/or
415 tooth mesowear analyses to assess the potential of resource partitioning between
416 *Haringtonhippus* and caballine *Equus* in the New World.
417

bioRxiv preprint doi: https://doi.org/10.1101/154963; this version posted June 24, 2017. The copyright holder for this preprint (which was not certified by peer review) is the author/funder. All rights reserved. No reuse allowed without permission.

418 **Fossil systematics in the palaeogenomics and proteomics era: concluding remarks**

419 Fossils of NWSL equids have been known for more than a century, but until the present study
420 their systematic position within Plio-Pleistocene Equidae was poorly characterized. This was not
421 because of a lack of interest on the part of earlier workers, whose detailed anatomical studies
422 strongly indicated that what we now call *Haringtonhippus* was related to Asiatic wild asses, such
423 as Tibetan khulan and Persian onagers, rather than to caballine horses (Eisenmann *et al*., 2008;
424 Guthrie, 2003; Scott, 2004; Skinner & Hibbard, 1972). That the cues of morphology have turned
425 out to be misleading in this case underlines a recurrent problem in systematic biology, which is
426 how best to discriminate authentic relationships within groups, such as Neogene equids, that
427 were prone to rampant convergence. The solution we adopted here was to utilize both
428 palaeogenomic and morphometric information in reframing the position of *Haringtonhippus*,
429 which now clearly emerges as the closest known outgroup to all living *Equus*.

430 Our success in this regard demonstrates that an approach which incorporates phenomics
431 with molecular methods (palaeogenomic as well as palaeoproteomic, e.g. (Welker et al., 2015))
432 is likely to offer a means for securely detecting relationships within speciose groups that are
433 highly diverse ecomorphologically. All methods have their limits, with taphonomic degradation
434 being the critical one for molecular approaches. However, proteins may persist significantly
435 longer than ancient DNA (e.g. (Rybczynski *et al*., 2013)), and collagen proteomics may come to
436 play a key role in characterizing affinities, as well as the reality, of several proposed Neogene
437 equine taxa (e.g. *Dinohippus*, *Pliohippus*, *Protohippus*, *Calippus*, and *Astrohippus*; (Macfadden,
438 1998)) whose distinctiveness and relationships are far from settled (Azzaroli & Voorhies, 1993;
439 Forsten, 1992). A reciprocally informative approach like the one taken here holds much promise
440 for lessening the amount of systematic noise, due to oversplitting, that hampers our

bioRxiv preprint doi: https://doi.org/10.1101/154963; this version posted June 24, 2017. The copyright holder for this preprint (which was not certified by peer review) is the author/funder. All rights reserved. No reuse allowed without permission.

441 understanding of the evolutionary biology of other major late Pleistocene megafaunal groups
442 such as bison and mammoths (Enk *et al*., 2016; Froese *et al*., 2017). This approach is clearly
443 capable of providing new insights into just how extensive megafaunal losses were at the end of
444 the Pleistocene, in what might be justifiably called the opening act of the Sixth Mass Extinction
445 in North America.
446

bioRxiv preprint doi: https://doi.org/10.1101/154963; this version posted June 24, 2017. The copyright holder for this preprint (which was not certified by peer review) is the author/funder. All rights reserved. No reuse allowed without permission.

Materials and Methods

We provide an overview of methods here; full details can be found in Appendix 1.

Sample collection and radiocarbon dating. We recovered Yukon fossil material (17 *Haringtonhippus francisci*, two *Equus* cf. *scotti*, and two *E. lambei*; Supplementary file 1) from active placer mines in the Klondike goldfields near Dawson City. We further sampled seven *H. francisci* fossils from the contiguous USA that are housed in collections at the University of Kansas Biodiversity Institute (KU; n=4), Los Angeles County Museum of Natural History (LACM(CIT); n=2), and the Texas Memorial Museum (TMM; n=1). We radiocarbon dated the Klondike fossils and the *H. francisci* cranium from the LACM(CIT) (Supplementary file 1).

Morphometric analysis of third metatarsals. For morphometric analysis, we took measurements of third metatarsals (MTIII) and other elements. We used a reduced data set of four MTIII variables for principal components analysis and performed logistic regression on the first three principal components, computed in R (R Development Core Team, 2008) (Supplementary file 6).

DNA extraction, library preparation, target enrichment, and sequencing. We conducted all molecular biology methods prior to indexing PCR in the dedicated palaeogenomics laboratory facilities at either the UC Santa Cruz or Pennsylvania State University. We extracted DNA from between 100 and 250 mg of bone powder following either (Rohland, Siedel, & Hofreiter, 2010) or (Dabney, *et al*., 2013). We then converted DNA extracts to libraries following the Meyer and Kircher protocol (Meyer & Kircher, 2010), as modified by (Heintzman *et al*., 2015) or the PSU

bioRxiv preprint doi: https://doi.org/10.1101/154963; this version posted June 24, 2017. The copyright holder for this preprint (which was not certified by peer review) is the author/funder. All rights reserved. No reuse allowed without permission.

method of (Vilstrup *et al*., 2013). We enriched libraries for equid mitochondrial DNA. We then sequenced all enriched libraries and unenriched libraries from 17 samples using Illumina platforms.

Mitochondrial genome reconstruction and analysis. We prepared raw sequence data for alignment and mapped the filtered reads to the horse reference mitochondrial genome (Genbank: NC_001640.1) and a *H. francisci* reference mtDNA genome (Genbank: KT168321), resulting in mitogenomic coverage ranging from 5.8× to 110.7× (Supplementary file 1). We were unable to recover equid mtDNA from TMM 34-2518 (the *francisci* holotype) using this approach (Appendix 2). We supplemented our mtDNA genome sequences with 38 previously published complete equid mtDNA genomes. We constructed six alignment data sets and selected models of molecular evolution for the analyses described below (Supplementary table 8, and Supplementary files 1 and 8).

We tested the phylogenetic position of the NWSL equids (=*H. francisci*) using mtDNA data sets 1-3 and applying Bayesian (Ronquist *et al*., 2012) and Maximum Likelihood (ML; (Stamatakis, 2014)) analyses. We varied the outgroup, the inclusion or exclusion of the fast-evolving partitions, and the inclusion or exclusion of *Hippidion* sequences. Due to the lack of a globally supported topology across the Bayesian and ML phylogenetic analyses, we used an Evolutionary Placement Algorithm (EPA; (Berger *et al*., 2011)) to determine the *a posteriori* likelihood of phylogenetic placements for candidate equid outgroups using mtDNA data set four. We also used the same approach to assess the placement of previously published equid sequences (Appendix 2). To infer divergence times between the four major equid groups (*Hippidion*, NWSL equids, caballine *Equus*, and non-caballine *Equus*), we ran Bayesian timetree

bioRxiv preprint doi: https://doi.org/10.1101/154963; this version posted June 24, 2017. The copyright holder for this preprint (which was not certified by peer review) is the author/funder. All rights reserved. No reuse allowed without permission.

493 analyses (Drummond *et al*. 2012) using mtDNA data set five. We varied these analyses by
494 including or excluding fast-evolving partitions, constrained the root height or not, and including
495 or excluding the *E. ovodovi* sequence.
496 To facilitate future identification of equid mtDNA sequences, we constructed, using data
497 set six, a list of putative synapomorphic base states, including indels and substitutions, that
498 define the genera *Hippidion*, *Haringtonhippus*, and *Equus* at sites across the mtDNA genome.
499
500 **Phylogenetic inference, divergence date estimation, and sex determination from nuclear**
501 **genomes.** To test whether our mtDNA genome-based phylogenetic hypothesis truly reflects the
502 species tree, we compared the nuclear genomes of a horse (EquCab2), donkey (Orlando *et al*.,
503 2013), and the shotgun sequence data from 17 of our NWSL equid samples (Appendix 1,
504 Appendix 1-figure 1 and Supplementary files 1-2). We applied four successive approaches,
505 which controlled for reference genome and DNA fragment length biases (Appendix 1).
506 We estimated the divergence between the NWSL equids and *Equus* (horse and donkey)
507 by fitting the branch length, or relative private transversion frequency, ratio between
508 horse/donkey and NWSL equids into a simple phylogenetic scenario (Figure 1-Figure
509 supplement 3). We then multiplied the NWSL equid branch length by a previous horse-donkey
510 divergence estimate (4.0-4.5 Ma; (Orlando *et al*., 2013)) to give the estimated NWSL equid-
511 *Equus* divergence date, following (Heintzman *et al*., 2015) and assuming a strict genome-wide
512 molecular clock (Figure 1-Figure supplement 3).
513 We determined the sex of the 17 NWSL equid samples by comparing the relative
514 mapping frequency of the autosomes to the X chromosome.
515

bioRxiv preprint doi: https://doi.org/10.1101/154963; this version posted June 24, 2017. The copyright holder for this preprint (which was not certified by peer review) is the author/funder. All rights reserved. No reuse allowed without permission.

516 **DNA damage analysis.** We assessed the prevalence of mitochondrial and nuclear DNA damage
517 in a subset of the equid samples using mapDamage (Jónsson *et al*., 2013).
518
519 **Data availability.** Repository details and associated metadata for curated samples can be found
520 in Supplementary file 1. MTIII and other element measurement data are in Supplementary file 4,
521 and the Rscript used for morphometric analysis is Supplementary file 6. MtDNA genome
522 sequences have been deposited in Genbank under accessions KT168317-KT168336, MF134655-
523 MF134663, and an updated version of JX312727. All mtDNA genome alignments and associated
524 XML and tree files are in Supplementary files 7-9. Raw shotgun sequence data used for the
525 nuclear genomic analyses have been deposited in the Short Read Archive (Bioproject:
526 PRJNA384940; SRA accessions: SRR5556842-SRR5556858).
527

bioRxiv preprint doi: https://doi.org/10.1101/154963; this version posted June 24, 2017. The copyright holder for this preprint (which was not certified by peer review) is the author/funder. All rights reserved. No reuse allowed without permission.

Appendix 1 Supplementary methods

1.1 Yukon sample context and identification

Pleistocene vertebrate fossils are commonly recovered at these localities, in the absence of stratigraphic context, as miners are removing frozen sediments to access underlying gold bearing gravel (Froese *et al*., 2009; Harington, 2011). We recovered *H. francisci* fossils along with other typical late Pleistocene (Rancholabrean) taxa, including caballine horses (*Equus* sp.), woolly mammoth (*Mammuthus primigenius*), steppe bison (*Bison priscus*), and caribou (*Rangifer tarandus*), which are consistent with our age estimates based on radiocarbon dating (Supplementary file 1). All Yukon fossil material consisted of limb bones that were taxonomically assigned based on their slenderness and are housed in the collections of the Yukon Government (YG).

1.2 Radiocarbon dating

We subsampled fossil specimens using handheld, rotating cutting tools and submitted them to either the KECK Accelerator Mass Spectrometry (AMS) Laboratory at the University of California (UC), Irvine (UCIAMS) and/or the Center for AMS (CAMS) at the Lawrence Livermore National Laboratory. We extracted collagen from the fossil subsamples using ultrafiltration (Beaumont, Beverly, Southon, & Taylor, 2010), which was used for AMS radiocarbon dating. We were unable to recover collagen from TMM 34-2518 (*francisci* holotype), consistent with the probable middle Pleistocene age of this specimen (Lundelius & Stevens, 1970). We recovered finite radiocarbon dates from all other fossils, with the exception of the two *Equus* cf. *scotti* specimens. We calibrated AMS radiocarbon dates using the IntCal13

bioRxiv preprint doi: https://doi.org/10.1101/154963; this version posted June 24, 2017. The copyright holder for this preprint (which was not certified by peer review) is the author/funder. All rights reserved. No reuse allowed without permission.

curve (Reimer *et al*., 2013) in OxCal v4.2 (https://c14.arch.ox.ac.uk/oxcal/OxCal.html) and report median calibrated dates in Supplementary file 1.

1.3 Morphometric analysis of third metatarsals

Third metatarsal (MTIII) and other elemental measurements were either taken by G.D.Z. or E.S. or from the literature (Supplementary file 4). For morphometric analysis, we focused exclusively on MTIIIs, which exhibit notable differences in slenderness among equid groups (Figure 2-Figure supplement 2a; (Weinstock *et al*., 2005)). Starting with a data set of 10 variables (following (Eisenmann, Alberdi, deGiuli, & Staesche, 1988)), we compared the loadings of all variables in principal components space in order to remove redundant measurements. This reduced the data set to four variables (GL: greatest length, Pb: proximal breadth, Mb: midshaft breadth, and DABm: distal articular breadth at midline). We visualized the reduced variables using principal components analysis, computed in R (Supplementary file 5; (R Development Core Team, 2008)), and performed logistic regression on the first three principal components to test whether MTIII morphology can distinguish stilt-legged (hemionine *Equus* and *H. francisci*, n=105) from stout-legged (caballine *Equus,* n=187) equid specimens.

1.4 Target enrichment and sequencing

We enriched libraries for equid mitochondrial DNA following the MyBaits v2 protocol (MYcroarray, Ann Arbor, MI), with RNA bait molecules constructed from the horse reference mitochondrial genome sequence (NC_001640.1). We then sequenced the enriched libraries for 2× 150 cycles on the Illumina HiSeq-2000 platform at UC Berkeley or 2× 75 cycles on the MiSeq platform at UC Santa Cruz, following the manufacturer's instructions. We produced data

bioRxiv preprint doi: https://doi.org/10.1101/154963; this version posted June 24, 2017. The copyright holder for this preprint (which was not certified by peer review) is the author/funder. All rights reserved. No reuse allowed without permission.

573 for the nuclear genomic analyses by shotgun sequencing 17 of the unenriched libraries for 2× 75
574 cycles on the MiSeq to produce ~1.1-6.4 million reads per library (Supplementary file 2).
575
576 **1.5 Mitochondrial genome reconstruction**
577 We initially reconstructed the mitochondrial genome for *H. francisci* specimen YG 404.663
578 (PH047). For sequence data enriched for the mitochondrial genome, we trimmed adapter
579 sequences, merged paired-end reads (with a minimum overlap of 15 base pairs (bp) required),
580 and removed merged reads shorter than 25 bp, using SeqPrep
581 (https://github.com/jstjohn/SeqPrep). We then mapped the merged and remaining unmerged
582 reads to the horse reference mitochondrial genome sequence using the Burrows-Wheeler Aligner
583 aln (BWA-aln v0.7.5; (Li & Durbin, 2010)), with ancient parameters (-l 1024; (Schubert *et al*.,
584 2012)). We removed reads with a mapping quality less than 20 and collapsed duplicated reads to
585 a single sequence using SAMtools v0.1.19 rmdup (Li *et al*., 2009). We called consensus
586 sequences using Geneious v8.1.7 (Biomatters, http://www.geneious.com; (Kearse *et al*., 2012)).
587 We then re-mapped the reads to the same reference mitochondrial genome using the iterative
588 assembler, MIA (Briggs *et al*., 2009). Consensus sequences from both alignment methods
589 required each base position to be covered a minimum of three times, with a minimum base
590 agreement of 67%. The two consensus sequences were then combined to produce a final
591 consensus sequence for YG 404.663 (Genbank: KT168321), which we used as the *H. francisci*
592 reference mitochondrial genome sequence.
593 For the remaining newly analyzed 21 *H. francisci*, two *E.* cf. *scotti*, and two *E. lambei*
594 samples, we merged and removed reads as described above. We then separately mapped the
595 retained reads to the horse and *H. francisci* mitochondrial reference genome sequences using

bioRxiv preprint doi: https://doi.org/10.1101/154963; this version posted June 24, 2017. The copyright holder for this preprint (which was not certified by peer review) is the author/funder. All rights reserved. No reuse allowed without permission.

MIA. Consensus sequences from MIA analyses were called as described above. The two consensus sequences were then combined to produce a final consensus sequence for each sample, with coverage ranging from 5.8× to 110.7× (Supplementary file 1). We also reconstructed the mitochondrial genomes for four previously published samples: YG 401.268, LACM(CIT) 109/150807, KU 62158, and KU 62055 (Supplementary file 1; (Vilstrup *et al*., 2013; Weinstock *et al*., 2005)).

1.6 Mitochondrial genome alignments

We supplemented our 30 new mitochondrial genome sequences with 38 previously published complete equid mitochondrial genomes, which included all extant *Equus* species, and extinct *Hippidion*, *E. ovodovi*, and *E.* cf. *scotti* ('equids'). We constructed six alignment data sets for the mitochondrial genome analyses: (1) equids and White rhinoceros (*Ceratotherium simum*; NC_001808) (n=69); (2) equids and Malayan tapir (*Tapirus indicus*; NC_023838) (n=69); (3) equids, six rhinos, two tapirs, and dog (*Canis lupus familiaris*; NC_002008) (n=77); (4) equids, six rhinos, two tapirs, ten published equid short fragments, and two published NWSL equid mitochondrial genome sequences (n=88); (5) a reduced equid data set (n=32); and (6) a full equid data set (n=68) (Supplementary file 8). For data sets three and four, we selected one representative from all rhino and tapir species for which full mitochondrial genome data are publicly available (Supplementary file 1).

For all six data sets, we first created an alignment using muscle (v3.8.31; (15)). We then manually scrutinized alignments for errors and removed a 253 bp variable number of tandem repeats (VNTR) part of the control region, corresponding to positions 16121-16373 of the horse reference mitochondrial genome. We partitioned the alignments into six partitions (three codon

bioRxiv preprint doi: https://doi.org/10.1101/154963; this version posted June 24, 2017. The copyright holder for this preprint (which was not certified by peer review) is the author/funder. All rights reserved. No reuse allowed without permission.

619 positions, ribosomal-RNAs, transfer-RNAs, and control region), using the annotated horse
620 reference mitochondrial genome in Geneious, following (Heintzman *et al*., 2015). We excluded
621 the fast-evolving control region alignment for data set three, which included the highly-diverged
622 dog sequence. For each partition, we selected models of molecular evolution using the Bayesian
623 information criterion in jModelTest (v2.1.6; (Darriba, Taboada, Doallo, & Posada, 2012))
624 (Supplementary table 8).
625

626 **1.7 Phylogenetic analysis of mitochondrial genomes**

627 To test the phylogenetic position of the NWSL equids, we conducted Bayesian and maximum
628 likelihood (ML) phylogenetic analyses of data sets one, two, and three, under the partitioning
629 scheme and selected models of molecular evolution described above. For outgroup, we selected:
630 White rhinoceros (data set one), Malayan tapir (data set two), or dog (data set three). For each of
631 the data sets, we varied the analyses based on (a) inclusion or exclusion of the fast-evolving
632 partitions (third codon positions and control region, where appropriate) and (b) inclusion or
633 exclusion of the *Hippidion* sequences. We ran Bayesian analyses in MrBayes (v3.2.6, (Ronquist
634 *et al*., 2012)) for two parallel runs of 10 million generations, sampling every 1,000, with the first
635 25% discarded as burn-in. We conducted ML analyses in RAxML (v8.2.4, (Stamatakis, 2014)),
636 using the GTRGAMMAI model across all partitions, and selected the best of three trees. We
637 evaluated branch support with both Bayesian posterior probability scores from MrBayes and 500
638 ML bootstrap replicates in RAxML.
639

640 **1.8 Placement of outgroups and published sequences *a posteriori***

bioRxiv preprint doi: https://doi.org/10.1101/154963; this version posted June 24, 2017. The copyright holder for this preprint (which was not certified by peer review) is the author/funder. All rights reserved. No reuse allowed without permission.

We used the Evolutionary Placement Algorithm (EPA) in RAxML to determine the *a posteriori* likelihood of phylogenetic placements for eight candidate equid outgroups (two tapirs, six rhinos) relative to the four well supported major equid groups (*Hippidion*, NWSL equids, caballine *Equus*, non-caballine *Equus*). We first constructed an unrooted reference tree consisting only of the equids from data set four in RAxML. We then analyzed the placements of the eight outgroups and retaining all placements up to a cumulative likelihood threshold of 0.99. We used the same approach to assess the placement of 12 previously published equid sequences derived from four NWSL equids (Vilstrup *et al*., 2013; Weinstock *et al*., 2005), five *Hippidion devillei* (Orlando *et al*., 2009), and three *E. ovodovi* (Orlando *et al*., 2009) (Supplementary table 4).

1.9 Divergence date estimation from mitochondrial genomes

To further investigate the topology of the four major equid groups, and to infer divergence times between them, we ran Bayesian timetree analyses in BEAST (v1.8.4; (Drummond *et al*., 2012)). Unlike the previous analyses, BEAST can resolve branching order in the absence of an outgroup, by using branch length and molecular clock methods. For BEAST analyses, we used data set five. We did not enforce monophyly. Where available, we used radiocarbon dates to tip date ancient samples. For two samples without available radiocarbon dates, we sampled the ages of tips. For the *E. ovodovi* sample (mtDNA genome: NC_018783), which was found in a cave that has been stratigraphically dated as late Pleistocene and includes other *E. ovodovi* remains have been dated to ~45-50 ka BP (Eisenmann & Sergej, 2011; Orlando *et al*., 2009), we used the following lognormal prior (mean: 4.5×10^4, log(stdev): 0.766, offset: 1.17×10^4) to ensure that 95% of the prior fell within the late Pleistocene (11.7-130 ka BP). For the *E.* cf. *scotti*

bioRxiv preprint doi: https://doi.org/10.1101/154963; this version posted June 24, 2017. The copyright holder for this preprint (which was not certified by peer review) is the author/funder. All rights reserved. No reuse allowed without permission.

mitochondrial genome (KT757763), we used a normal prior (mean: 6.7×10^5, stdev: 5.64×10^4) to ensure that 95% of the prior fell within the proposed age range of this specimen (560-780 ka BP; (Orlando *et al*., 2013)). We further calibrated the tree using an age of 4-4.5 Ma for the root of crown group *Equus* (normal prior, mean 4.25×10^6, stdev: 1.5×10^5) (Orlando *et al*., 2013). To assess the impact of variables on the topology and divergence times, we either (a) included or excluded the fast-evolving partitions, (b) constrained the root height (lognormal prior: mean 1×10^7, stdev: 1.0) or not, and (c) included or excluded the *E. ovodovi* sequence, which was not directly dated. We used the models of molecular evolution estimated by jModeltest (Supplementary table 8). We estimated the substitution and clock parameters for each partition, and estimated a single tree using all partitions. We implemented the birth-death serially sampled (BDSS) tree prior. We ran two analyses for each variable combination. In each analysis, we ran the MCMC chain for 100 million generations, sampling trees and parameters every 10,000, and discarding the first 10% as burn-in. We checked log files for convergence in Tracer (v1.6; http://tree.bio.ed.ac.uk/software/tracer/). We combined trees from the two runs for each variable combination in LogCombiner (v1.8.4) and then calculated the maximum clade credibility (MCC) tree in TreeAnnotator (v1.8.4). We report divergence dates as 95% highest posterior probability credibility intervals of node heights.

1.10 Mitochondrial synapomorphy analysis

We first divided data set six, which consists of all available and complete equid mitogenomic sequences, into three data sets based on the genera *Hippidion*, *Haringtonhippus*, and *Equus*. For each of the three genus-specific alignments, we created a strict consensus sequence, whereby sites were only called if there was 100% sequence agreement, whilst including gaps and

bioRxiv preprint doi: https://doi.org/10.1101/154963; this version posted June 24, 2017. The copyright holder for this preprint (which was not certified by peer review) is the author/funder. All rights reserved. No reuse allowed without permission.

687 excluding ambiguous sites. We then compared the three genus-specific consensus sequences to
688 determine sites where one genus exhibited a base state that is different to the other two genera,
689 or, at five sites, where each genus has its own base state (Supplementary file 5). In this analysis,
690 we did not make any inference regarding the ancestral state for the identified synapomorphic
691 base states. We identified 391 putative mtDNA genome synapomorphies for *Hippidion*, 178 for
692 *Haringtonhippus*, and 75 for *Equus* (Supplementary file 5).
693
694 **1.11 Phylogenetic inference from nuclear genomes**
695 We compared the genomes of a horse (*E. caballus*; EquCab2; GCA_000002305.1) and donkey
696 (*E. asinus*; Willy, 12.4×; http://geogenetics.ku.dk/publications/middle-pleistocene-omics;
697 (Orlando *et al*., 2013)) with shotgun sequence data from 17 of our NWSL equid samples
698 (Supplementary files 1-2). We merged paired-end reads using SeqPrep as described above,
699 except that we removed merged reads shorter than 30 bp. We further removed merged and
700 remaining unmerged reads that had low sequence complexity, defined as a DUST score >7, using
701 PRINSEQ-lite v0.20.4 (Schmieder & Edwards, 2011). We used four successive approaches to
702 minimize the impact of mapping bias introduced from ancient DNA fragment length variation
703 and reference genome choice.
704 We first followed a modified version of the approach outlined in (Heintzman *et al*.,
705 2015). We mapped the donkey genome to the horse genome by computationally dividing the
706 donkey genome into 150 bp 'pseudo-reads' tiled every 75 bp, and aligned these pseudo-reads
707 using Bowtie2-local v2.1.0 (Langmead & Salzberg, 2012) while allowing one seed mismatch
708 and a maximum mismatch penalty of four to better account for ancient DNA specific damage
709 (Appendix 1-figure 1, steps 1-3). We then mapped the filtered shotgun data from each of the

bioRxiv preprint doi: https://doi.org/10.1101/154963; this version posted June 24, 2017. The copyright holder for this preprint (which was not certified by peer review) is the author/funder. All rights reserved. No reuse allowed without permission.

NWSL equid samples to the horse genome using Bowtie2-local with the settings described above, and removed PCR duplicated reads and those with a mapping quality score of <30 in SAMtools. We called a pseudo-haploidized sequence for the donkey and NWSL equid alignments, by randomly picking a base with a base quality score ≥60 at each position, using SAMtools mpileup. We masked positions that had a coverage not equal to 2× (donkey) or 1× (NWSL equid), and those located on scaffolds shorter than 100 kb (Appendix 1-figure 1, step 4). As the horse, donkey, and NWSL equid genome sequences were all based on the horse genome coordinates, we compared the relative transversion frequency between the donkey or NWSL equids and the horse using custom scripts. We restricted our analyses to transversions to avoid the impacts of ancient DNA damage, which can manifest as erroneous transitions from the deamination of cytosine (e.g. Appendix 2-Figures 1-2) (Dabney, Meyer, & Pääbo, 2013). We repeated this analysis, but with the horse and NWSL equids mapped to the donkey genome (the donkey genome coordinate framework).

bioRxiv preprint doi: https://doi.org/10.1101/154963; this version posted June 24, 2017. The copyright holder for this preprint (which was not certified by peer review) is the author/funder. All rights reserved. No reuse allowed without permission.

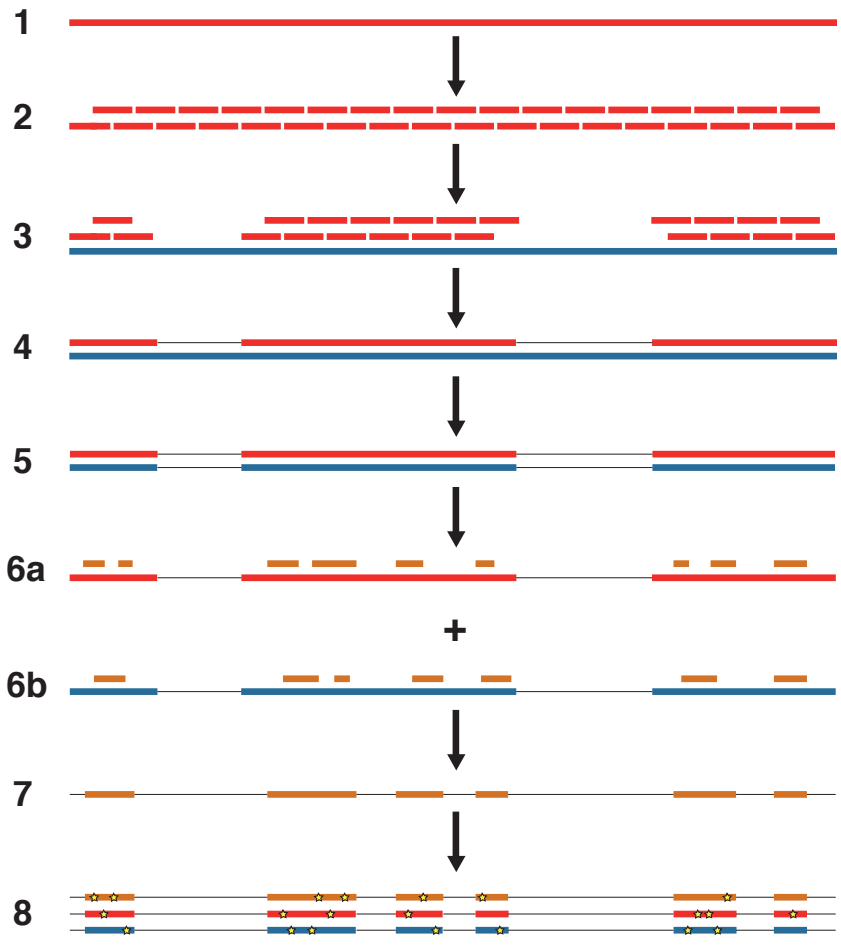

Appendix 1-Figure 1. An overview of the nuclear genome analysis pipeline. A first reference genome sequence (red; step 1) is divided into 150 bp pseudo-reads, tiled every 75 bp for exactly 2× genomic coverage (step 2). These pseudo-reads are then mapped to a second reference genome (blue; step 3), and a consensus sequence of the mapped pseudo-reads is called (step 4). Regions of the second reference genome that are not covered by the pseudo-reads are masked (step 5). For each NWSL equid sample, reads (orange) are mapped independently to the first reference consensus sequence (step 6a) and masked second reference genome (step 6b). Alignments from steps 6a and 6b are then merged (step 7). For alignment coordinates that have base calls for the first reference, second reference, and NWSL equid sample genomes, the relative frequencies of private transversion substitutions (yellow stars) for each genome are

bioRxiv preprint doi: https://doi.org/10.1101/154963; this version posted June 24, 2017. The copyright holder for this preprint (which was not certified by peer review) is the author/funder. All rights reserved. No reuse allowed without permission.

735 calculated (step 8). The co-ordinates from the second reference genome (blue) are used for each
736 analysis.
737
738 For the second approach and using the horse genome coordinate framework, we next
739 masked sites in the horse reference genome that were not covered by donkey reads at a depth of
740 2×. This resulted in the horse genome and donkey consensus sequence being masked at the same
741 positions (Appendix 1-figure 1, step 5). We then separately mapped the filtered NWSL equid
742 shotgun data to scaffolds longer than 100 kb for the masked horse genome and donkey consensus
743 sequence (Appendix 1-figure 1, step 6), called NWSL equid consensus sequences, and calculated
744 relative transversion frequencies as described above. This analysis was repeated using the
745 donkey genome coordinate framework.
746 Next, for each genome coordinate framework, we combined the two alignments for each
747 NWSL equid sample from approach two to create a union of reads mappable to both the masked
748 coordinate genome and alternate genome consensus sequence (Appendix 1-figure 1, step 7). If a
749 NWSL equid read mapped to different coordinates between the two references, we selected the
750 alignment with the higher map quality score and randomly selected between mappings of equal
751 quality. We then called NWSL equid consensus sequences as above. As this third approach
752 allowed for simultaneous comparison of the horse, donkey, and NWSL equid sequences, we
753 calculated relative private transversion frequencies for each sequence, at sites where all three
754 sequences had a base call, using tri-aln-report (https://github.com/Paleogenomics/Chrom-
755 Compare) (Appendix 1-figure 1, step 8).
756 Finally, as a fourth approach and for both genome coordinate frameworks, we repeated
757 approach three with the exception that we divided the NWSL alignments by mapped read length.

bioRxiv preprint doi: https://doi.org/10.1101/154963; this version posted June 24, 2017. The copyright holder for this preprint (which was not certified by peer review) is the author/funder. All rights reserved. No reuse allowed without permission.

We split the alignments into 10 bp read bins ranging from 30-39 to 120-129 bp, and discarded longer reads and paired-end reads that were unmerged by SeqPrep. We called consensus sequences and calculated relative private transversion frequencies for each sequence as described above. We only used relative private transversion frequencies from the 90-99 to 120-129 bp bins for divergence date estimates (Appendix 2).

1.12 Sex determination from nuclear genomes

We used the alignments of the 17 NWSL equids to the horse genome, from approach one described above, to infer the probable sex of these individuals. For this, we determined the number of reads mapped to each chromosome using SAMtools idxstats. For each chromosome, we then calculated the relative mapping frequency by dividing the number of mapped reads by the length of the chromosome. We then compared the relative mapping frequency between the autosomes and X-chromosome. As males and females are expected to have one and two copies of the X chromosome, respectively, and two copies of every autosome, we inferred a male if the ratio between the autosomes and X-chromosome was 0.45-0.55 and a female if the ratio were 0.9-1.1.

1.13 DNA damage analysis

For a subset of nine samples, we realigned the filtered sequence data from the libraries enriched for equid mitochondrial DNA to either the *H. francisci* (for *H. francisci* samples) or horse (for *E. lambei* and *E.* cf. *scotti* samples) reference mitochondrial genome sequences using BWA-aln as described above. We also realigned the filtered unenriched sequence data to the horse reference

bioRxiv preprint doi: https://doi.org/10.1101/154963; this version posted June 24, 2017. The copyright holder for this preprint (which was not certified by peer review) is the author/funder. All rights reserved. No reuse allowed without permission.

780 genome (EquCab2) for a subset of six samples using the same approach. We then analyzed

781 patterns of DNA damage in mapDamage v2.0.5 (Jónsson *et al*., 2013).

782

bioRxiv preprint doi: https://doi.org/10.1101/154963; this version posted June 24, 2017. The copyright holder for this preprint (which was not certified by peer review) is the author/funder. All rights reserved. No reuse allowed without permission.

Appendix 2 Supplementary Results

2.1 Ancient DNA characterization

We selected a subset of samples for the analysis of DNA damage patterns. In all of these samples, we observe expected patterns of damage in both mitochondrial and nuclear DNA, including evidence of the deamination of cytosine residues at the ends of reads, depurination-induced strand breaks, and a short mean DNA fragment length (Dabney, Meyer, & Pääbo, 2013) (Appendix 2-Figures 1-2). We note that the sample with the greatest proportion of deaminated cytosines is *E*. cf. *scotti* (YG 198.1; Appendix 2-Figure 1v-x), which is the oldest sample in the subset (Supplementary file 1).

bioRxiv preprint doi: https://doi.org/10.1101/154963; this version posted June 24, 2017. The copyright holder for this preprint (which was not certified by peer review) is the author/funder. All rights reserved. No reuse allowed without permission.

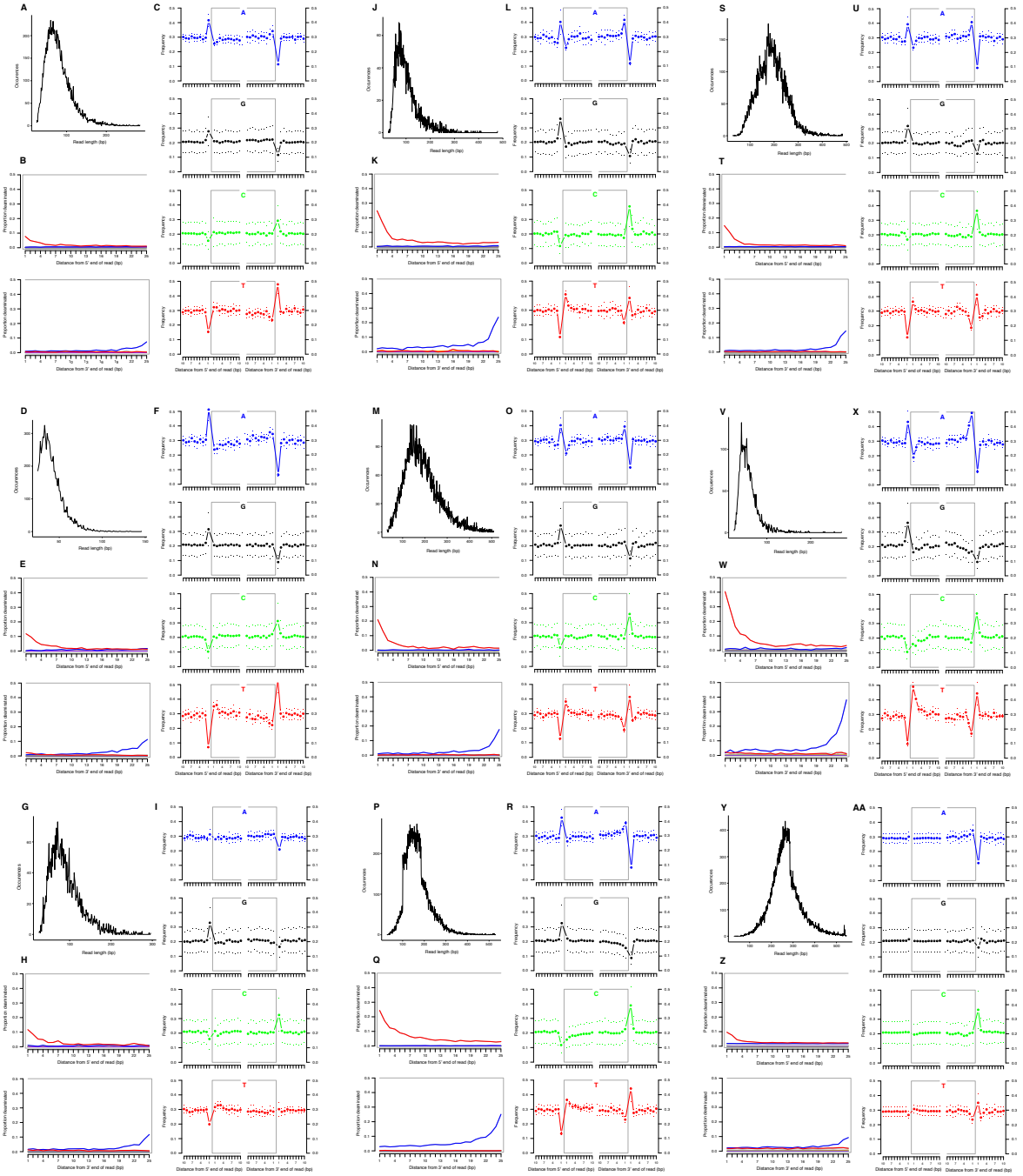

793

794 **Appendix 2-Figure 1.** Characterization of ancient mitochondrial DNA damage patterns from

795 nine equid samples. *H. francisci*: (A-C) JK166 (LACM(CIT) 109/150807; Nevada), (D-F) JK207

796 (LACM(CIT) 109/156450; Nevada), (G-I) JK260 (KU 47800; Wyoming), (J-L) PH013 (YG

797 130.6; Yukon), (M-O) PH047 (YG 404.663; Yukon), (P-R) MS272 (YG 401.268; Yukon), (S-U)

bioRxiv preprint doi: https://doi.org/10.1101/154963; this version posted June 24, 2017. The copyright holder for this preprint (which was not certified by peer review) is the author/funder. All rights reserved. No reuse allowed without permission.

798 MS349 (YG 130.55; Yukon); *E.* cf. *scotti*: (V-X) PH055 (YG 198.1; Yukon); *E. lambei*: (Y-AA)
799 MS316 (YG 328.54; Yukon). Every third panel: (A) to (Y) DNA fragment length distributions;
800 (B) to (Z) proportion of cytosines that are deaminated at fragment ends (red: cytosine →
801 thymine; blue: guanine → adenine); and (C) to (AA) mean base frequencies immediately
802 upstream and downstream of the 5' and 3' ends of mapped reads.
803

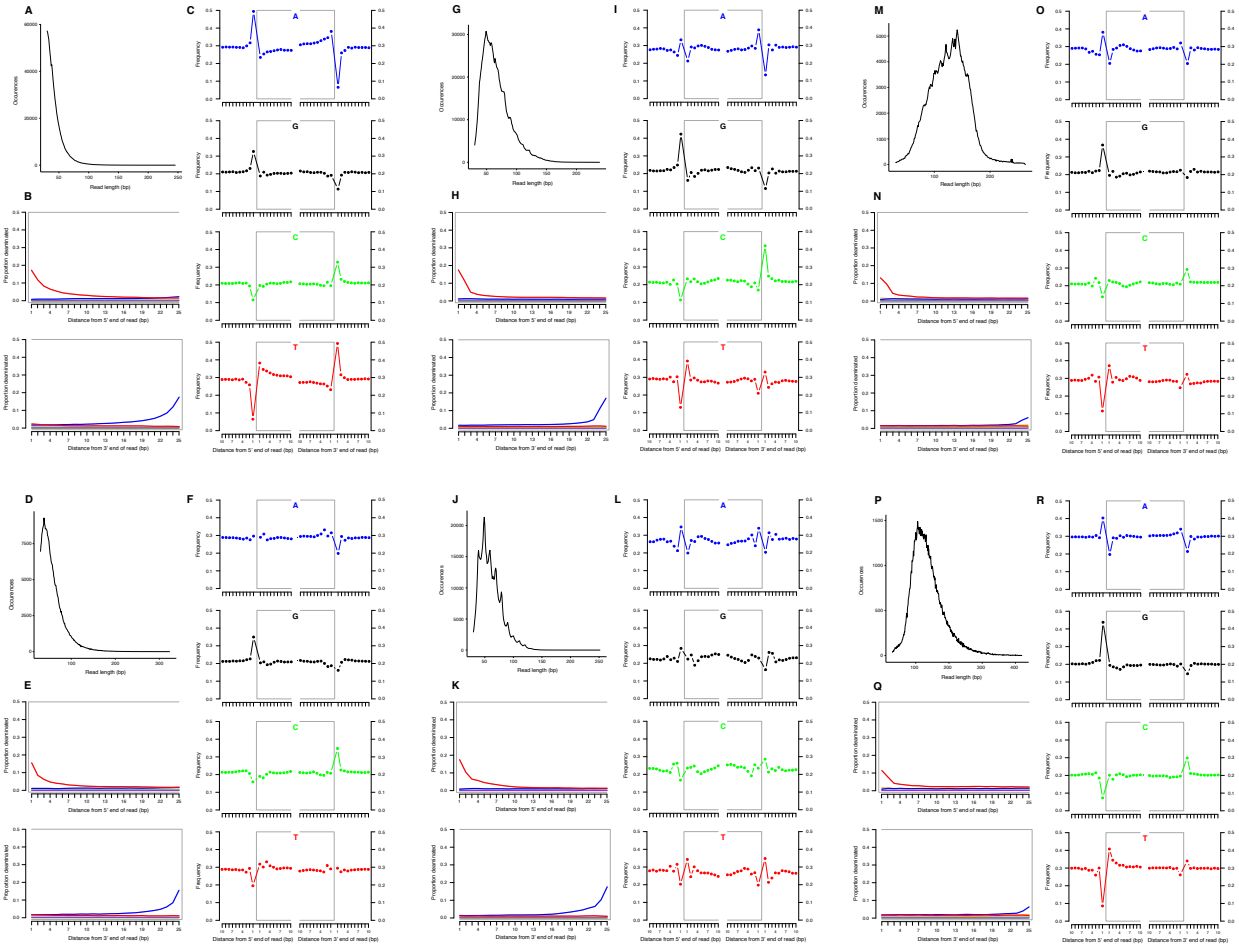

804

805 **Appendix 2-Figure 2.** Characterization of ancient nuclear DNA damage patterns from six *H.*
806 *francisci* samples. (A-C) JK166 (LACM(CIT) 109/150807; Nevada), (D-F) JK260 (KU 47800;
807 Wyoming), (G-I) PH013 (YG 130.6; Yukon), (J-L) PH036 (YG 76.2; Yukon), (M-O) MS349
808 (YG 130.55; Yukon), (P-R) MS439 (YG 401.387; Yukon). Every third panel: (A) to (P) DNA

bioRxiv preprint doi: https://doi.org/10.1101/154963; this version posted June 24, 2017. The copyright holder for this preprint (which was not certified by peer review) is the author/funder. All rights reserved. No reuse allowed without permission.

fragment length distributions; (B) to (Q) proportion of cytosines that are deaminated at fragment ends (red: cytosine → thymine; blue: guanine → adenine); and (C) to (R) mean base frequencies immediately upstream and downstream of the 5' and 3' ends of mapped reads.

2.2 Resolving the phylogenetic placement of NWSL equids using mitochondrial genomes

We ran Bayesian and ML phylogenetic analyses on mtDNA genome alignment data sets 1-3, whilst varying the outgroup, including (all) or excluding (reduced) the fast-evolving partitions (see Appendix 1), and including or excluding the *Hippidion* sequences. In all analyses, we recover four major equid groups (*Hippidion*, NWSL equids(=*H. francisci*), caballine *Equus*, and non-caballine *Equus*) with strong statistical support (Bayesian posterior probability (BPP): 1.000; ML bootstrap: 96-100%; Supplementary table 1), consistent with previous studies (e.g. (Der Sarkissian *et al*., 2015; Orlando *et al*., 2009)). We recover conflicting phylogenetic topologies between these four groups, however, which is dependent on the variables described above and the choice of phylogenetic algorithm (Appendix 2-Figure 3; Supplementary table 1). Across all analyses, strong statistical support (BPP: ≥0.99; ML bootstrap: ≥95%) is only associated with topology 1 (Appendix 2-Figure 3; Supplementary table 1), in which NWSL equids are placed outside of *Equus*, and *Hippidion* is placed outside of the NWSL equid-*Equus* clade. We note that the analyses with the strongest support consist of multiple outgroups (mtDNA data set three).

bioRxiv preprint doi: https://doi.org/10.1101/154963; this version posted June 24, 2017. The copyright holder for this preprint (which was not certified by peer review) is the author/funder. All rights reserved. No reuse allowed without permission.

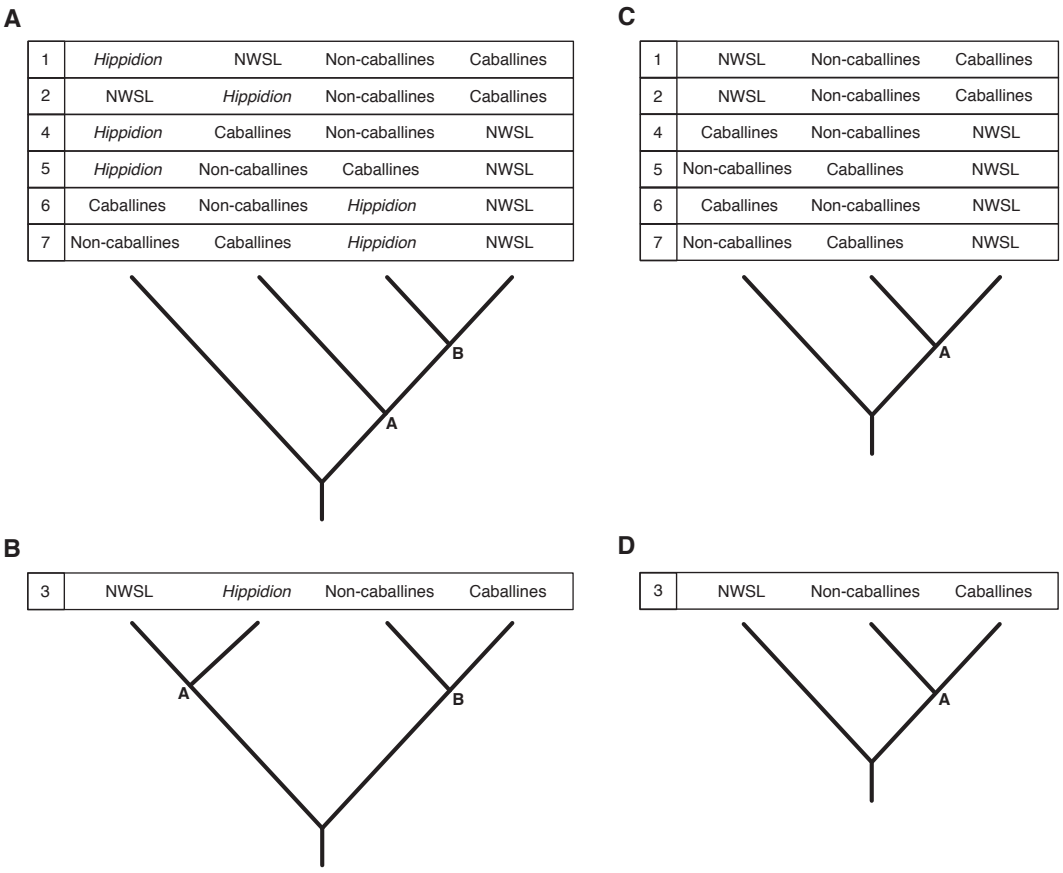

829

830 **Appendix 2-Figure 3.** Seven phylogenetic hypotheses for the four major groups of equids with
831 sequenced mitochondrial genomes: *Hippidion*, the New World stilt-legged equids
832 (=*Haringtonhippus*), non-caballine *Equus* (asses, zebras, and *E. ovodovi*) and caballine *Equus*
833 (horses). (A) imbalanced and (B) balanced hypotheses. The hypotheses presented in (C) and (D)
834 are identical to (A) and (B), except that *Hippidion* is excluded. Node letters are referenced in
835 Supplementary tables 1-2. We only list combinations that were recovered by our palaeogenomic,
836 or previous palaeogenetic, analyses

837

838 We further investigated the effect of outgroup choice by using an evolutionary placement
839 algorithm (EPA; (Berger *et al*., 2011)) to place the outgroup sequences into an unrooted ML
840 phylogeny *a posteriori* using the same set of variables described above. We find that the

bioRxiv preprint doi: https://doi.org/10.1101/154963; this version posted June 24, 2017. The copyright holder for this preprint (which was not certified by peer review) is the author/funder. All rights reserved. No reuse allowed without permission.

outgroup placement likelihood is increased with the inclusion of *Hippidion* sequences, and that the only placements with a likelihood of ≥0.95 are consistent with topology one (Appendix 2-Figure 3; Supplementary table 2), in agreement with the Bayesian and ML phylogenetic analyses. The phylogenetic and EPA analyses demonstrate that outgroup choice can greatly impact equid phylogenetic inference and that multiple outgroups should be used for resolving relationships between major equid groups.

We lastly ran Bayesian timetree analyses in BEAST in the absence of an outgroup, whilst including or excluding the fast-evolving partitions, including or excluding the *E. ovodovi* sequence, and constraining the root prior or not. All BEAST analyses yielded a maximum clade credibility tree that is consistent with topology one (Figures 1 and S11) with BPP support for the NWSL equid-*Equus* and *Equus* clades of 0.996-1.000 (Supplementary table 3). Altogether, the phylogenetic, EPA, and timetree analyses support topology one (Appendix 2-Figure 3), with NWSL equids falling outside of *Equus*, and therefore the NWSL equids as a separate genus, *Haringtonhippus*.

2.3 Placement of previously published NWSL equid sequences

To confirm that all six previously published NWSL equid samples with available mtDNA sequence data (Vilstrup *et al*., 2013; Weinstock *et al*., 2005) belong to *H. francisci*, we either reconstructed mitochondrial genomes for these samples (JW277, JW161; (Weinstock *et al*., 2005)), placed the sequences into a ML phylogeny *a posteriori* using the EPA whilst varying the partitioning scheme and inclusion or exclusion of *Hippidion* (Supplementary table 4), or both. For JW277 and JW161, the mitochondrial genomes were consistent with those derived from the newly analyzed samples (Figure 1-Figure supplement 1). For three other NWSL equid

bioRxiv preprint doi: https://doi.org/10.1101/154963; this version posted June 24, 2017. The copyright holder for this preprint (which was not certified by peer review) is the author/funder. All rights reserved. No reuse allowed without permission.

mitochondrial sequences (JW125, JW126, and JW328; (Vilstrup *et al*., 2013; Weinstock *et al*., 2005)), including one sample from Mineral Hill cave (Supplementary file 1), the EPA strongly supported a ML placement within the *H. francisci* clade (cumulative likelihood of 0.995-1.000). However, the EPA placed the remaining NWSL equid sample (MS272; (Vilstrup *et al*., 2013)) on the branch leading to *H. francisci* with strong support (likelihood: 1.000; Supplementary table 4). We therefore explored whether the published sequence for MS272 is problematic.

We first tested the EPA on eight other equid mitochondrial sequences (*E. ovodovi*, n=3; *Hippidion devillei*, n=5), which grouped as expected from previous analyses (likelihood: 0.999-1.000; Supplementary table 4; (Orlando *et al*., 2009)). We then used our mitochondrial genome assembly pipeline to reconstruct a consensus for MS272 from the raw data used by (Vilstrup *et al*., 2013), which resulted in a different sequence that was consistent with other NWSL equids. To confirm this new sequence, we used the original MS272 DNA extract for library preparation, target enrichment, and sequencing. The consensus from this analysis was identical to our new sequence.

We sought to understand the origins of the problems associated with the published MS272 sequence. We first applied our synapomorphy analysis. For the called bases, we found that the published MS272 sequence contained 0/384 diagnostic bases for *Hippidion*, 124/164 for *Haringtonhippus*, and 16/70 for *Equus* (Supplementary file 5). We infer from this analysis that the published MS272 sequence is therefore ~76% *Haringtonhippus* and that ~23% originates from *Equus*. The presence of *Equus* synapomorphies could be explained by the fact that the enriched library for MS272 was sequenced on the same run as ancient caballine horses (*Equus*), thereby potentially introducing contaminating reads from barcode bleeding (Kircher, Sawyer, & Meyer, 2012), which may have been exacerbated by alignment to the modern horse reference

bioRxiv preprint doi: https://doi.org/10.1101/154963; this version posted June 24, 2017. The copyright holder for this preprint (which was not certified by peer review) is the author/funder. All rights reserved. No reuse allowed without permission.

887 mitochondrial genome with BWA-aln and consensus calling using SAMtools (Vilstrup *et al*.,
888 2013). The presence of caballine horse sequence in the published MS272 mtDNA genome
889 explains why previous phylogenetic analyses of mitochondrial genomes have recovered NWSL
890 equids as sister to caballine *Equus* with strong statistical support (Der Sarkissian *et al*., 2015;
891 Vilstrup *et al*., 2013).
892

893 **2.4 Resolving the phylogenetic placement of NWSL equids using nuclear genomes**
894 The horse and donkey genomes are representative of total *Equus* genomic diversity (Jónsson *et*
895 *al*., 2014), and so, if NWSL equids are *Equus*, we should expect their genomes to be more
896 similar to either horse or donkey than to the alternative.
897 Initial analyses based on approach one (see Appendix 1) were inconclusive, with some
898 NWSL equid samples appearing to fall outside of *Equus* (higher relative transversion frequency
899 between the NWSL equid and the horse or donkey than between the horse and donkey) and
900 others inconsistently placed in the phylogeny, appearing most closely related to horse when
901 aligned to the horse genome and most closely related donkey when aligned to the donkey
902 genome (Supplementary file 2). We then used approaches two and three in an attempt to
903 standardize between the horse and donkey reference genomes, and therefore reduce potential
904 bias introduced from the reference genome. In the latter union-based approach, mapping should
905 not be disproportionately sensitive to regions of the genome where NWSL equids are more
906 horse- or donkey-like. These approaches, however, were not successful, but we noted that
907 relative (private) transversion frequency for the coordinate genome and NWSL equid sequences
908 correlated with mean DNA fragment length (Appendix 2-Figure 4 and Supplementary file 2). We
909 therefore used approach four to control for the large variation in mean DNA fragment length

bioRxiv preprint doi: https://doi.org/10.1101/154963; this version posted June 24, 2017. The copyright holder for this preprint (which was not certified by peer review) is the author/funder. All rights reserved. No reuse allowed without permission.

between NWSL equid sequences (Appendix 2-Figure 2 and Supplementary file 2), which is likely due to a combination of DNA preservation and differences in the DNA extraction and library preparation techniques used (Supplementary file 2). This allowed for direct comparison between the NWSL equid samples, which showed a consistent pattern across read length bins (Figure 1-Figure supplement 2, Supplementary table 3). The relative private transversion frequency for both the coordinate genome and NWSL equid sequences increase with read length until the 90-99 bp bin, at which point the coordinate genome and alternate sequence relative private transversion frequencies converge (defined as a ratio between 0.95-1.05) and the NWSL equid relative private transversion frequencies reach plateau at between 1.40-1.56× greater than that of the horse or donkey (Figure 1-Figure supplements 2-3, Supplementary table 3).

A greater relative private transversion frequency in NWSL equids, as compared to horse and donkey, is consistent with their being more diverged than the horse-donkey split (*Equus*) and therefore supports the hypothesis of NWSL equids as a separate genus (*Haringtonhippus*).

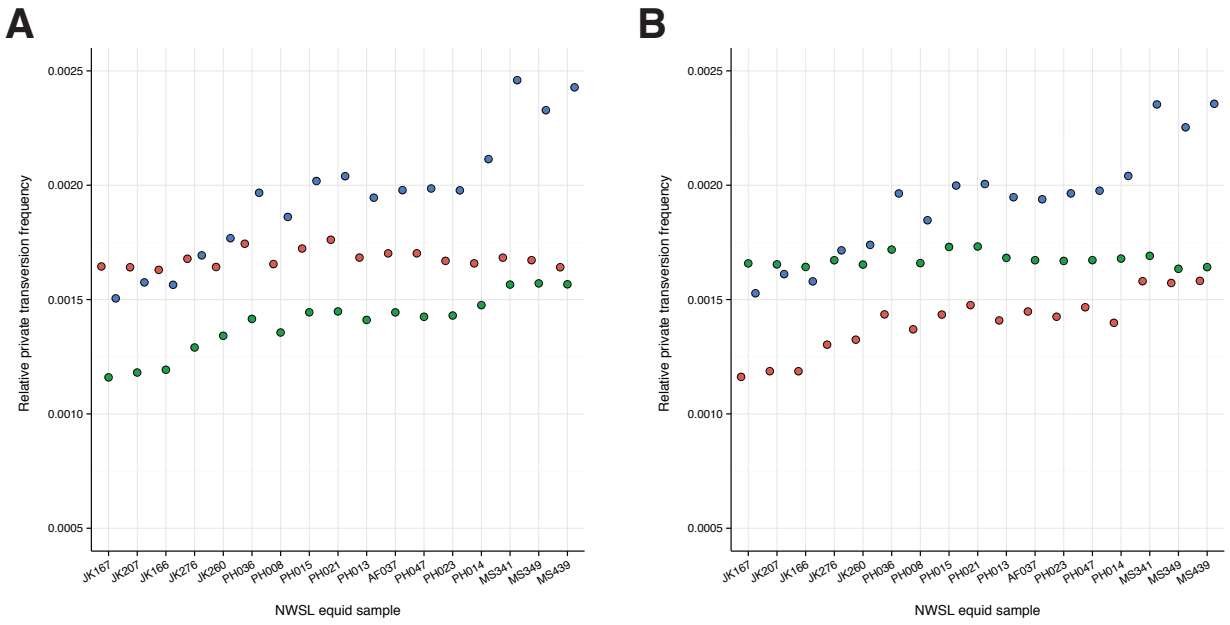

bioRxiv preprint doi: https://doi.org/10.1101/154963; this version posted June 24, 2017. The copyright holder for this preprint (which was not certified by peer review) is the author/funder. All rights reserved. No reuse allowed without permission.

925 **Appendix 2-Figure 4.** A comparison of relative private transversion frequencies between the
926 nuclear genomes of a caballine *Equus* (horse, *E. caballus*; green), a non-caballine *Equus*
927 (donkey, *E. asinus*; red), and the 17 New World-stilt legged (NWSL) equid samples
928 (=*Haringtonhippus francisci*; blue), using approach three (Appendix 1), with samples ordered by
929 increasing mean mapped read length. Analyses are based on alignment to the horse (A) or
930 donkey (B) genome coordinates.
931

932 **2.5 Sex determination from nuclear genomes**

933 We inferred the sex of our 17 NWSL equid samples by calculating the ratio of relative mapping
934 frequencies between the autosomes and X-chromosome (Supplementary file 3). We find that five
935 of our samples are male and at least eight are female (Supplementary table 6). We note that all
936 three Gypsum Cave samples are inferred to be female, have statistically indistinguishable
937 radiocarbon dates, and identical mtDNA genome sequences (Figure 1-Figure supplement 1b,
938 Supplementary file 1). We therefore cannot reject the possibility that these samples derive from
939 the same individual. Intriguingly, we further note that, across all 17 NWSL equid samples, the
940 relative mapping frequency for chromosomes 8 and 13 is appreciably greater than the remaining
941 autosomes (Supplementary file 3). This may suggest that duplicated regions of these
942 chromosomes are present in NWSL equids, as compared to the horse (*E. caballus*).
943

944 **2.6 Designation of a type species for *Haringtonhippus***

945 We sought to designate a type species for the NWSL equid genus, *Haringtonhippus*, using an
946 existing name, in order to avoid adding to the unnecessarily extensive list of Pleistocene North
947 American equid species names (Winans, 1985). For this, we scrutinized eight names that have

bioRxiv preprint doi: https://doi.org/10.1101/154963; this version posted June 24, 2017. The copyright holder for this preprint (which was not certified by peer review) is the author/funder. All rights reserved. No reuse allowed without permission.

948 previously been assigned to NWSL equids in order of priority (date the name was first described
949 in the literature). We rejected names that were solely based on dentitions, as these anatomical
950 features are insufficient for delineating between equid groups (Groves & Willoughby, 1981). The
951 earliest named species with a valid, diagnostic holotype is *francisci* Hay 1915. On the basis of
952 taxonomic priority, stratigraphic age, and cranial and metatarsal comparisons (see main results
953 and below), we conclude that *francisci* Hay 1915 is the most appropriate name for
954 *Haringtonhippus*. We also note that this middle Pleistocene species is also small, like our late
955 Pleistocene specimens.
956 The eight examined names were:
957 ***tau*** Owen, 1869: a small species erected based upon an upper cheek tooth series lacking the P^2
958 from the Valley of Mexico. Other than small size, the species has no reliably diagnostic features.
959 The holotype specimen has been lost, and no topotypal material is available, and so determining
960 whether or not the species represents a NWSL equid is impossible. Eisenmann and colleagues
961 (2008) proposed a neotype specimen for the species, consisting of a cranium (FC 673), but this is
962 rejected here on technical grounds: 1) the proposed neotype fossil was listed as being part of a
963 private collection, which negates its use as a neotype; 2) ICZN rules require that a neotype be
964 "consistent with what is known of the former name-bearing type from the original description
965 and from other sources" and derive from “as nearly as practicable from the original type locality
966 … and, where relevant, from the same geological horizon or host species as the original name-
967 bearing type”.
968 ***semiplicatus*** Cope, 1893: based upon an isolated upper molar tooth from Rock Creek, Texas.
969 The specimen has been interpreted to be derived from the same species as the holotype

bioRxiv preprint doi: https://doi.org/10.1101/154963; this version posted June 24, 2017. The copyright holder for this preprint (which was not certified by peer review) is the author/funder. All rights reserved. No reuse allowed without permission.

970 metatarsal of '*E*'. *calobatus* Troxell (see below) (Azzaroli, 1995; Quinn, 1957; Sandom, Faurby,
971 Sandel, & Svenning, 2014).
972 ***littoralis*** Hay, 1913: based upon an upper cheek tooth from Peace Creek, Florida. The tooth is
973 small, but offers no diagnostic features.
974 ***francisci*** Hay, 1915: Named in April of 1915 based upon a partial skeleton, including the skull,
975 mandible, and a broken MTIII (TMM 34-2518). Confidently determined to be a NWSL equid
976 based upon reconstruction of the right MTIII by Lundelius and Stevens (1970).
977 ***calobatus*** Troxell, 1915: Named in June of 1915 based upon limb bones. No holotype
978 designated, but lectotype erected by Hibbard (1953) (YPM 13470, right MTIII).
979 ***altidens*** Quinn, 1957: based upon a partial skeleton from Blanco Creek, Texas that exhibits
980 elongate metapodials. Synonymized with *francisci* Hay by Winans (1985).
981 ***zoyatalis*** Mooser, 1958: based upon a partial mandible including the symphyseal region and the
982 right dentary with p2-m3. Synonymized with *francisci* Hay by Winans (1985).
983 ***quinni*** Slaughter *et al*. 1962: based upon a MTIII (SMP 60578) and other referred elements from
984 Texas. Synonymized with *francisci* Hay by Lundelius and Stevens (1970) and Winans (1985).
985

986 **2.7 Anatomical comparison of the *francisci* holotype and Gypsum Cave crania**
987 We compared the holotype of *francisci* Hay (TMM 34-2518) from Texas to the Gypsum Cave
988 cranium (LACM(CIT) 109/156450) from Nevada, the latter of which was assigned to
989 *Haringtonhippus* using palaeogenomic data (Figure 2-Figure supplement 1). Although there are
990 minor anatomical differences between the two crania, which are outlined below, we consider
991 these to fall within the range of intraspecific variation.

bioRxiv preprint doi: https://doi.org/10.1101/154963; this version posted June 24, 2017. The copyright holder for this preprint (which was not certified by peer review) is the author/funder. All rights reserved. No reuse allowed without permission.

The skull from Gypsum Cave (GCS) can be distinguished from that of the *francisci* holotype (*f*HS) by its slightly larger size, and markedly longer and more slender rostrum, both absolutely and as a percentage of the skull length. The rostrum of the GCS is also absolutely narrower; the *f*HS, despite being the smaller skull, is transversely broader at the i/3. The palatine foramina are positioned medial to the middle of the M^2 in the GCS, whereas they are medial to the M^2-M^3 junction in the *f*HS. Viewed laterally, the orbits of the GCS have more pronounced supraorbital ridges than those of the *f*HS. The latter skull also exhibits somewhat stronger basicranial flexion than the GCS. Dentally, the GCS exhibits arcuate protocones, with strong anterior heels and marked lingual troughs in P^3-M^3; the *f*HS has smaller, triangular protocones with less pronounced anterior heels and no lingual trough or groove. These characters are not thought to result from different ontogenetic stages, since both specimens appear to be of young adults (all teeth in wear and tall in the jaw). Both the GCS and the *f*HS have relatively simple enamel patterns on the cheek teeth, with few evident plications. Not only are the observed differences between these two specimens unlikely to result from ontogeny, they also don't result from sex, since both skulls appear to be females given the absence of canine teeth. The inference of the GCS being female is further supported by palaeogenomic data (Supplementary table 6).

2.8 Attempt to recover DNA from the *francisci* holotype

We attempted to retrieve endogenous mitochondrial and nuclear DNA from the holotype of *francisci* Hay (TMM 34-2518), to directly link this anatomically-derived species name with our palaeogenomically-derived genus name *Haringtonhippus*, but were unsuccessful.

After sequencing a library enriched for equid mitochondrial DNA (see Appendix 1), we could only align 11 reads to the horse reference mitochondrial genome sequence with BWA.

bioRxiv preprint doi: https://doi.org/10.1101/154963; this version posted June 24, 2017. The copyright holder for this preprint (which was not certified by peer review) is the author/funder. All rights reserved. No reuse allowed without permission.

Using the basic local alignment search tool (BLASTn), we show that these reads are 100% match to human and therefore likely originate from contamination. We repeated this approach using MIA and aligned 166 reads, which were concentrated in 20 regions of the mitochondrial genome. We identified these sequences as human (n=18, 96-100% identity), cow (n=1, 100%), or Aves (n=1, 100%), consistent with the absence of endogenous mitochondrial DNA in this sample.

We further generated ~800,000 reads from the unenriched library for TMM 34-2518, and followed a modified metagenomic approach, outlined in (Graham *et al*., 2016), to assess if any endogenous DNA was present. We mapped the reads to the horse reference genome (EquCab2), using the BWA-aln settings of (Graham *et al*., 2016), of which 538 reads aligned. We then compared these aligned reads to the BLASTn database. None of the reads uniquely hit Equidae or had a higher score to Equidae than non-Equidae, whereas 492 of the reads either uniquely hit non-Equidae or had a higher score to non-Equidae than Equidae. These results are consistent with either a complete lack, or an ultra-low occurrence, of endogenous DNA in TMM 34-2518.

2.9 Morphometric analysis of third metatarsals

Stilt- and stout-legged equids can be distinguished with high accuracy (98.2%; logistic regression) on the basis of third metatarsal (MTIII) morphology (Figure 2c, and Supplementary files 3 and 5), which has the potential to easily and confidently distinguish candidates from either group prior to more costly genetic testing. We note that future genetic analysis of ambiguous specimens, that cross the 'middle ground' between stilt- and stout-legged regions of morphospace, could open the possibility of a simple length-vs-width definition for these two morphotypes. Furthermore, we can highlight potential misidentifications, such as the two putative *E. lambei* specimens that fall within stilt-legged morphospace (Figure 2c), which could

bioRxiv preprint doi: https://doi.org/10.1101/154963; this version posted June 24, 2017. The copyright holder for this preprint (which was not certified by peer review) is the author/funder. All rights reserved. No reuse allowed without permission.

1038 then be tested by genetic analysis. Intriguingly, an Old World *E. ovodovi* (stilt-legged; MT no. 6;
1039 (Eisenmann & Sergej, 2011))) and New World *E. scotti* (stout-legged; CMN 29867) specimen
1040 directly overlap in a stout-legged region of morphospace (Figure 2c), which could indicate that
1041 either this *E. ovodovi* specimen was misidentified or that this species straddles the delineation
1042 between stilt- and stout-legged morphologies.

1043 *H. francisci* occupies a region of morphospace distinct from caballine/stout-legged
1044 *Equus*, but overlaps considerably with hemionine/stilt-legged *Equus* (Figure 2c). The holotype of
1045 *H. francisci* (TMM 34-2518) is very pronounced in its slenderness; it has a greater MTIII length
1046 than most other *H. francisci* but slightly smaller width/breadth measurements. This holotype is
1047 surpassed in these dimensions only by the *quinni* Slaughter *et al*. holotype, which has itself
1048 previously been synonymized with *francisci* Hay (Lundelius & Stevens, 1970; Winans, 1985).
1049 This suggests a potentially larger range of MTIII morphology for *H. francisci* than exhibited by
1050 the presently assigned specimens. We observe that this diversity may be influenced by
1051 geography, with *H. francisci* specimens from high-latitude Beringia having shorter MTIIIs
1052 relative to those from the lower-latitude contiguous USA.

1053 We note that two New World caballine *Equus* from Yukon, *E.* cf. *scotti* and *E. lambei*,
1054 appear to separate in morphospace (Figure 2c), primarily by MTIII length, supporting the
1055 potential delineation of these two taxa using MTIII morphology alone.
1056

bioRxiv preprint doi: https://doi.org/10.1101/154963; this version posted June 24, 2017. The copyright holder for this preprint (which was not certified by peer review) is the author/funder. All rights reserved. No reuse allowed without permission.

Acknowledgements

We thank the Klondike placer gold mining community of Yukon for their support and providing access to their mines from which many of our *Haringtonhippus* fossils were recovered. We thank Matt Brown and Chris Sagebiel of the Texas Vertebrate Palaeontology Collections at the University of Texas, Austin for access to a portion of TMM 34-2518, and also thank Sam McLeod, Vanessa Rhue, and Aimee Montenegro at the Los Angeles County Museum for access to the Gypsum Cave material for consumptive sampling. Thanks to Brent Breithaupt (Bureau of Land Management) for permitting the sampling of fossils from Natural Trap Cave that were originally recovered by Larry Martin, Miles Gilbert, and colleagues, and are presently curated by the University of Kansas Biodiversity Institute. We thank Chris Beard and David Burnham (University of Kansas) for facilitating access to these fossils. Thanks to Tom Guilderson, Andrew Fields, Dan Chang, and Samuel Vohr for technical assistance. Thanks to Greger Larson for providing the base map in Figure 1. We thank two anonymous reviewers whose comments improved this manuscript. This work used the Vincent J. Coates Genomics Sequencing Laboratory at UC Berkeley, supported by NIH S10 Instrumentation Grants S10RR029668 and S10RR027303. PDH, JAC, MS, and BS were supported by NSF grants PLR-1417036 and 09090456. LO was supported by the Danish Council for Independent Research Natural Sciences (Grant 4002-00152B); the Danish National Research Foundation (Grant); the “Chaires d'Attractivit. 2014” IDEX, University of Toulouse, France (OURASI), and the European Research Council (ERC-CoG-2015-681605).

Competing interests

The authors declare no competing interests.

bioRxiv preprint doi: https://doi.org/10.1101/154963; this version posted June 24, 2017. The copyright holder for this preprint (which was not certified by peer review) is the author/funder. All rights reserved. No reuse allowed without permission.

References

Allen, W. R., & Short, R. V. (1997). Interspecific and extraspecific pregnancies in equids: anything goes. *The Journal of Heredity*, *88*(5), 384–392.

Azzaroli, A. (1992). Ascent and decline of monodactyl equids: a case for prehistoric overkill. *Annales Zoologici Fennici*, *28*(3-4), 151–163.

Azzaroli, A. (1995). A synopsis of the Quaternary species of *Equus* in North America. *Bolletino Della Societa Palaeontologica Italiana*, *34*(2), 205–221.

Azzaroli, A., & Voorhies, M. R. (1993). The Genus *Equus* in North America. The Blancan species. *Palaeontographia Italica*, *80*, 175–198.

Beaumont, W., Beverly, R., Southon, J., & Taylor, R. E. (2010). Bone preparation at the KCCAMS laboratory. *Nuclear Instruments & Methods in Physics Research. Section B, Beam Interactions with Materials and Atoms*, *268*(7-8), 906–909.

Bennett, E. A., Champlot, S., Peters, J., Arbuckle, B. S., Guimaraes, S., Pruvost, M., … Geigl, E.-M. (2017). Taming the Late Quaternary phylogeography of the Eurasiatic wild ass through ancient and modern DNA. *PLoS One*, *12*(4), e0174216.

Berger, S. A., Krompass, D., & Stamatakis, A. (2011). Performance, accuracy, and Web server for evolutionary placement of short sequence reads under maximum likelihood. *Systematic Biology*, *60*(3), 291–302.

Briggs, A. W., Good, J. M., Green, R. E., Krause, J., Maricic, T., Stenzel, U., … Pääbo, S. (2009). Targeted retrieval and analysis of five Neandertal mtDNA genomes. *Science*, *325*(5938), 318–321.

bioRxiv preprint doi: https://doi.org/10.1101/154963; this version posted June 24, 2017. The copyright holder for this preprint (which was not certified by peer review) is the author/funder. All rights reserved. No reuse allowed without permission.

1101 Burke, A., Eisenmann, V., & Ambler, G. K. (2003). The systematic position of *Equus*
1102 *hydruntinus,* an extinct species of Pleistocene equid☆. *Quaternary Research*, *59*(3), 459–
1103 469.
1104 Clark, P. U., Dyke, A. S., Shakun, J. D., Carlson, A. E., Clark, J., Wohlfarth, B., … McCabe, A.
1105 M. (2009). The Last Glacial Maximum. *Science*, *325*(5941), 710–714.
1106 Dabney, J., Knapp, M., Glocke, I., Gansauge, M.-T., Weihmann, A., Nickel, B., … Meyer, M.
1107 (2013). Complete mitochondrial genome sequence of a Middle Pleistocene cave bear
1108 reconstructed from ultrashort DNA fragments. *Proceedings of the National Academy of*
1109 *Sciences of the United States of America*, *110*(39), 15758–15763.
1110 Dabney, J., Meyer, M., & Pääbo, S. (2013). Ancient DNA damage. *Cold Spring Harbor*
1111 *Perspectives in Biology*, *5*(7). https://doi.org/10.1101/cshperspect.a012567
1112 Darriba, D., Taboada, G. L., Doallo, R., & Posada, D. (2012). jModelTest 2: more models, new
1113 heuristics and parallel computing. *Nature Methods*, *9*(8), 772.
1114 Der Sarkissian, C., Vilstrup, J. T., Schubert, M., Seguin-Orlando, A., Eme, D., Weinstock, J., …
1115 Orlando, L. (2015). Mitochondrial genomes reveal the extinct *Hippidion* as an outgroup to
1116 all living equids. *Biology Letters*, *11*(3), 20141058–20141058.
1117 Drummond, A. J., Suchard, M. A., Xie, D., & Rambaut, A. (2012). Bayesian phylogenetics with
1118 BEAUti and the BEAST 1.7. *Molecular Biology and Evolution*, *29*(8), 1969–1973.
1119 Edgar, R. C. (2004). MUSCLE: multiple sequence alignment with high accuracy and high
1120 throughput. *Nucleic Acids Research*, *32*(5), 1792–1797.
1121 Eisenmann, V. (1985). Indications paléoécologiques fournies par les *Equus* (Mammalia,
1122 Perissodactyla) plio-pléistocènes d'Afrique. In *L'Environnement des Hominidés au Plio-*
1123 *Pléistocène* (pp. 57–79).

bioRxiv preprint doi: https://doi.org/10.1101/154963; this version posted June 24, 2017. The copyright holder for this preprint (which was not certified by peer review) is the author/funder. All rights reserved. No reuse allowed without permission.

1124 Eisenmann, V. (1992). Origins, dispersals, and migrations of *Equus* (Mammalia, Perissodactyla).
1125 *CFS Courier Forschungsinstitut Senckenberg*, *153*, 161–170.
1126 Eisenmann, V. (2003). Gigantic Horses. In A. Petculescu & E. Stiuca (Eds.), *Advances in*
1127 *Palaeontology "Hen to Panta", Papers in Honour of C. Radulescu and P. M. Samson* (pp.
1128 31–40). Bucharest.
1129 Eisenmann, V., Alberdi, M. T., deGiuli, C., & Staesche, U. (1988). Volume 1: methodology. In
1130 M. Woodburne & P. Sondaar (Eds.), *Studying Fossil Horses* (pp. 1–71). E. J. Brill, Leiden.
1131 Eisenmann, V., Howe, J., & Pichardo, M. (2008). Old world hemiones and new world slender
1132 species (Mammalia, Equidae). *Palaeovertebrata*, *36*(1-4), 159–233.
1133 Eisenmann, V., & Sergej, V. (2011). Unexpected finding of a new *Equus* species (Mammalia,
1134 Perissodactyla) belonging to a supposedly extinct subgenus in late Pleistocene deposits of
1135 Khakassia (Southwestern Siberia). *Geodiversitas*, *33*(3), 519–530.
1136 Enk, J., Devault, A., Widga, C., Saunders, J., Szpak, P., Southon, J., … Poinar, H. (2016).
1137 *Mammuthus* population dynamics in Late Pleistocene North America: divergence,
1138 phylogeography, and introgression. *Frontiers in Ecology and Evolution*, *4*.
1139 https://doi.org/10.3389/fevo.2016.00042
1140 Forsten, A. (1988). Middle Pleistocene replacement of stenonid horses by caballoid horses —
1141 ecological implications. *Palaeogeography, Palaeoclimatology, Palaeoecology*, *65*(1-2), 23–
1142 33.
1143 Forsten, A. (1992). Mitochondrial-DNA time-table and the evolution of *Equus*: comparison of
1144 molecular and palaeontological evidence. *Annales Zoologici Fennici*, *28*(3-4), 301–309.
1145 Forsten, A. (1996). Climate and the evolution of *Equus* (Perissodactyla, Equidae) in the Plio-
1146 Pleistocene of Eurasia. *Acta Zoologica Cracoviensia*, *39*(1), 161–166.

bioRxiv preprint doi: https://doi.org/10.1101/154963; this version posted June 24, 2017. The copyright holder for this preprint (which was not certified by peer review) is the author/funder. All rights reserved. No reuse allowed without permission.

1147 Froese, D. G., Stiller, M., Heintzman, P. D., Reyes, A. V., Zazula, G. D., Soares, A. E. R., …
1148 Shapiro, B. (2017). New fossil and genomic evidence constrains the timing of bison arrival
1149 in North America. *Proceedings of the National Academy of Sciences of the United States of*
1150 *America*, *114*(13), 3457–3462.
1151 Froese, D. G., Zazula, G. D., Westgate, J. A., Preece, S. J., Sanborn, P. T., Reyes, A. V., &
1152 Pearce, N. J. G. (2009). The Klondike goldfields and Pleistocene environments of Beringia.
1153 *GSA Today: A Publication of the Geological Society of America*, *19*(8), 4.
1154 Goebel, T., Waters, M. R., & O'Rourke, D. H. (2008). The late Pleistocene dispersal of modern
1155 humans in the Americas. *Science*, *319*(5869), 1497–1502.
1156 Graham, R. W., Belmecheri, S., Choy, K., Culleton, B. J., Davies, L. J., Froese, D., … Wooller,
1157 M. J. (2016). Timing and causes of mid-Holocene mammoth extinction on St. Paul Island,
1158 Alaska. *Proceedings of the National Academy of Sciences of the United States of America*,
1159 *113*(33), 9310–9314.
1160 Groves, C. P., & Willoughby, D. P. (1981). Studies on the taxonomy and phylogeny of the genus
1161 *Equus*. 1. Subgeneric classification of the recent species. *Mammalia*, *45*(3).
1162 https://doi.org/10.1515/mamm.1981.45.3.321
1163 Guthrie, R. D. (2003). Rapid body size decline in Alaskan Pleistocene horses before extinction.
1164 *Nature*, *426*(6963), 169–171.
1165 Guthrie, R. D. (2006). New carbon dates link climatic change with human colonization and
1166 Pleistocene extinctions. *Nature*, *441*(7090), 207–209.
1167 Harington, C. R. (2011). Pleistocene vertebrates of the Yukon Territory. *Quaternary Science*
1168 *Reviews*, *30*(17-18), 2341–2354.

bioRxiv preprint doi: https://doi.org/10.1101/154963; this version posted June 24, 2017. The copyright holder for this preprint (which was not certified by peer review) is the author/funder. All rights reserved. No reuse allowed without permission.

1169 Harington, C. R., & Clulow, F. V. (1973). Pleistocene Mammals from Gold Run Creek, Yukon
1170 Territory. *Canadian Journal of Earth Sciences*, *10*(5), 697–759.
1171 Hay, O. P. (1915). Contributions to the knowledge of the mammals of the Pleistocene of North
1172 America. *Proceedings of the United States National Museum*, *48*(2086), 515–575.
1173 Heintzman, P. D., Zazula, G. D., Cahill, J. A., Reyes, A. V., MacPhee, R. D. E., & Shapiro, B.
1174 (2015). Genomic data from extinct North American *Camelops* revise camel evolutionary
1175 history. *Molecular Biology and Evolution*, *32*(9), 2433–2440.
1176 Hibbard, C. W. (1953). *Equus* (*Asinus*) *calobatus* Troxell and associated vertebrates from the
1177 Pleistocene of Kansas. *Transactions of the Kansas Academy of Science. Kansas Academy of*
1178 *Science*, *56*(1), 111.
1179 Jónsson, H., Ginolhac, A., Schubert, M., Johnson, P. L. F., & Orlando, L. (2013).
1180 mapDamage2.0: fast approximate Bayesian estimates of ancient DNA damage parameters.
1181 *Bioinformatics* , *29*(13), 1682–1684.
1182 Jónsson, H., Schubert, M., Seguin-Orlando, A., Ginolhac, A., Petersen, L., Fumagalli, M., …
1183 Orlando, L. (2014). Speciation with gene flow in equids despite extensive chromosomal
1184 plasticity. *Proceedings of the National Academy of Sciences of the United States of America*,
1185 *111*(52), 18655–18660.
1186 Kearse, M., Moir, R., Wilson, A., Stones-Havas, S., Cheung, M., Sturrock, S., … Drummond, A.
1187 (2012). Geneious Basic: an integrated and extendable desktop software platform for the
1188 organization and analysis of sequence data. *Bioinformatics* , *28*(12), 1647–1649.
1189 Kircher, M., Sawyer, S., & Meyer, M. (2012). Double indexing overcomes inaccuracies in
1190 multiplex sequencing on the Illumina platform. *Nucleic Acids Research*, *40*(1), e3.

bioRxiv preprint doi: https://doi.org/10.1101/154963; this version posted June 24, 2017. The copyright holder for this preprint (which was not certified by peer review) is the author/funder. All rights reserved. No reuse allowed without permission.

1191 Koch, P. L., & Barnosky, A. D. (2006). Late Quaternary extinctions: state of the debate. *Annual*
1192 *Review of Ecology, Evolution, and Systematics*, *37*(1), 215–250.
1193 Langmead, B., & Salzberg, S. L. (2012). Fast gapped-read alignment with Bowtie 2. *Nature*
1194 *Methods*, *9*(4), 357–359.
1195 Li, H., & Durbin, R. (2010). Fast and accurate long-read alignment with Burrows-Wheeler
1196 transform. *Bioinformatics* , *26*(5), 589–595.
1197 Li, H., Handsaker, B., Wysoker, A., Fennell, T., Ruan, J., Homer, N., … 1000 Genome Project
1198 Data Processing Subgroup. (2009). The Sequence Alignment/Map format and SAMtools.
1199 *Bioinformatics* , *25*(16), 2078–2079.
1200 Lundelius, E. L., & Stevens, M. S. (1970). *Equus francisci* Hay, a Small Stilt-Legged Horse,
1201 Middle Pleistocene of Texas. *Journal of Palaeontology*, *44*(1), 148–153.
1202 Macdonald, M. L., & Toohey, L. M. (1992). *The Species, Genera, and Tribes of the Living and*
1203 *Extinct Horses of the World 1758-1966: From the Work of Morris F. Skinner*.
1204 MacFadden, B. J. (1992). *Fossil horses: systematics, palaeobiology, and evolution of the family*
1205 *Equidae*. Cambridge University Press.
1206 Macfadden, B. J. (1998). Equidae. In *Evolution of Tertiary Mammals of North America* (pp. 537–
1207 559).
1208 Meyer, M., & Kircher, M. (2010). Illumina sequencing library preparation for highly multiplexed
1209 target capture and sequencing. *Cold Spring Harbor Protocols*, *2010*(6), db.prot5448.
1210 O'Dea, A., Lessios, H. A., Coates, A. G., Eytan, R. I., Restrepo-Moreno, S. A., Cione, A. L., …
1211 Jackson, J. B. C. (2016). Formation of the Isthmus of Panama. *Science Advances*, *2*(8),
1212 e1600883.

bioRxiv preprint doi: https://doi.org/10.1101/154963; this version posted June 24, 2017. The copyright holder for this preprint (which was not certified by peer review) is the author/funder. All rights reserved. No reuse allowed without permission.

1213 Orlando, L., Ginolhac, A., Zhang, G., Froese, D., Albrechtsen, A., Stiller, M., … Willerslev, E.
1214 (2013). Recalibrating *Equus* evolution using the genome sequence of an early Middle
1215 Pleistocene horse. *Nature*, *499*(7456), 74–78.
1216 Orlando, L., Male, D., Alberdi, M. T., Prado, J. L., Prieto, A., Cooper, A., & Hänni, C. (2008).
1217 Ancient DNA clarifies the evolutionary history of American Late Pleistocene equids.
1218 *Journal of Molecular Evolution*, *66*(5), 533–538.
1219 Orlando, L., Mashkour, M., Burke, A., Douady, C. J., Eisenmann, V., & Hänni, C. (2006).
1220 Geographic distribution of an extinct equid (*Equus hydruntinus*: Mammalia, Equidae)
1221 revealed by morphological and genetical analyses of fossils. *Molecular Ecology*, *15*(8),
1222 2083–2093.
1223 Orlando, L., Metcalf, J. L., Alberdi, M. T., Telles-Antunes, M., Bonjean, D., Otte, M., …
1224 Cooper, A. (2009). Revising the recent evolutionary history of equids using ancient DNA.
1225 *Proceedings of the National Academy of Sciences of the United States of America*, *106*(51),
1226 21754–21759.
1227 Quinn, J. H. (1957). Pleistocene Equidae of Texas. *Bureau of Economic Geology, University of*
1228 *Texas, Report of Investigations*, *33*, 1–51.
1229 R Development Core Team. (2008). *R: A language and environment for statistical computing*.
1230 Retrieved from R Foundation for Statistical Computing, Vienna, Austria. ISBN 3-900051-
1231 07-0, URL http://www.R-project.org.
1232 Reimer, P. J., Bard, E., Bayliss, A., Beck, J. W., Blackwell, P. G., Bronk Ramsey, C., … van der
1233 Plicht, J. (2013). IntCal13 and Marine13 radiocarbon age calibration curves 0–50,000 years
1234 cal BP. *Radiocarbon*, *55*(4), 1869–1887.

bioRxiv preprint doi: https://doi.org/10.1101/154963; this version posted June 24, 2017. The copyright holder for this preprint (which was not certified by peer review) is the author/funder. All rights reserved. No reuse allowed without permission.

1235 Rohland, N., Siedel, H., & Hofreiter, M. (2010). A rapid column-based ancient DNA extraction
1236 method for increased sample throughput. *Molecular Ecology Resources*, *10*(4), 677–683.
1237 Ronquist, F., Teslenko, M., van der Mark, P., Ayres, D. L., Darling, A., Höhna, S., …
1238 Huelsenbeck, J. P. (2012). MrBayes 3.2: efficient Bayesian phylogenetic inference and
1239 model choice across a large model space. *Systematic Biology*, *61*(3), 539–542.
1240 Rybczynski, N., Gosse, J. C., Harington, C. R., Wogelius, R. A., Hidy, A. J., & Buckley, M.
1241 (2013). Mid-Pliocene warm-period deposits in the High Arctic yield insight into camel
1242 evolution. *Nature Communications*, *4*, 1550.
1243 Ryder, O. A., Epel, N. C., & Benirschke, K. (1978). Chromosome banding studies of the
1244 Equidae. *Cytogenetics and Cell Genetics*, *20*(1-6), 332–350.
1245 Sandom, C., Faurby, S., Sandel, B., & Svenning, J.-C. (2014). Global late Quaternary megafauna
1246 extinctions linked to humans, not climate change. *Proceedings. Biological Sciences / The*
1247 *Royal Society*, *281*(1787). https://doi.org/10.1098/rspb.2013.3254
1248 Schmieder, R., & Edwards, R. (2011). Quality control and preprocessing of metagenomic
1249 datasets. *Bioinformatics* , *27*(6), 863–864.
1250 Schubert, M., Ginolhac, A., Lindgreen, S., Thompson, J. F., Al-Rasheid, K. A. S., Willerslev, E.,
1251 … Orlando, L. (2012). Improving ancient DNA read mapping against modern reference
1252 genomes. *BMC Genomics*, *13*, 178.
1253 Scott, E. (2004). Pliocene and Pleistocene Horses from Porcupine Cave. In *Biodiversity Response*
1254 *to Climate Change in the Middle Pleistocene* (pp. 264–279).
1255 Skinner, M. F., & Hibbard, C. W. (1972). Early Pleistocene pre-glacial and glacial rocks and
1256 faunas of North-Central Nebraska. *Bulletin of the American Museum of Natural History*,
1257 *148*, 1–148.

bioRxiv preprint doi: https://doi.org/10.1101/154963; this version posted June 24, 2017. The copyright holder for this preprint (which was not certified by peer review) is the author/funder. All rights reserved. No reuse allowed without permission.

1258 Stamatakis, A. (2014). RAxML version 8: a tool for phylogenetic analysis and post-analysis of
1259 large phylogenies. *Bioinformatics*, *30*(9), 1312–1313.
1260 Steiner, C. C., & Ryder, O. A. (2013). Characterization of *Prdm9* in equids and sterility in mules.
1261 *PloS One*, *8*(4), e61746.
1262 Vilstrup, J. T., Seguin-Orlando, A., Stiller, M., Ginolhac, A., Raghavan, M., Nielsen, S. C. A., …
1263 Orlando, L. (2013). Mitochondrial phylogenomics of modern and ancient equids. *PloS One*,
1264 *8*(2), e55950.
1265 Weinstock, J., Willerslev, E., Sher, A., Tong, W., Ho, S. Y. W., Rubenstein, D., … Cooper, A.
1266 (2005). Evolution, systematics, and phylogeography of Pleistocene horses in the new world:
1267 a molecular perspective. *PLoS Biology*, *3*(8), e241.
1268 Welker, F., Collins, M. J., Thomas, J. A., Wadsley, M., Brace, S., Cappellini, E., … MacPhee, R.
1269 D. E. (2015). Ancient proteins resolve the evolutionary history of Darwin's South American
1270 ungulates. *Nature*, *522*(7554), 81–84.
1271 Winans, M. C. (1985). Revision of North American fossil species of the genus *Equus*
1272 (Mammalia: Perissodactyla: Equidae). Dissertation, Univ. of Texas, Austin. 264 pp.
1273 Zazula, G. D., MacPhee, R. D. E., Metcalfe, J. Z., Reyes, A. V., Brock, F., Druckenmiller, P. S.,
1274 … Southon, J. R. (2014). American mastodon extirpation in the Arctic and Subarctic
1275 predates human colonization and terminal Pleistocene climate change. *Proceedings of the*
1276 *National Academy of Sciences of the United States of America*, *111*(52), 18460–18465.
1277

Supplementary tables 1-8

Supplementary table 1. Topological shape and support values for the best supported trees from the Bayesian and Maximum likelihood (ML) analyses of mtDNA data sets 1-3, including either the all or reduced partition sets, and with *Hippidion* sequences either included or excluded.

Outgroup	Partitions	*Hippidion*?	Tips	MrBayes							RAxML						
				Topology	Support						Topology	Support					
					Node A	Node B	*Hippidion*	NWSL	NCs	Caballines		Node A	Node B	*Hippidion*	NWSL	NCs	Caballines
White rhino (Data set 1)	All	Excluded	63	**1 / 2 / 3**	**0.996***	N/A	N/A	1.000	1.000	1.000	1 / 2 / 3	71*	N/A	N/A	100	99	100
		Included	69	2	0.751	**1.000***	1.000	1.000	1.000	1.000	1	64*	**96***	100	100	100	100
	Reduced	Excluded	63	**1 / 2 / 3**	**1.000***	N/A	N/A	1.000	1.000	1.000	1 / 2 / 3	**100***	N/A	N/A	99	100	100
		Included	69	2	0.948	**1.000***	1.000	1.000	1.000	1.000	2	73	**98***	100	99	100	100
Malayan tapir (Data set 2)	All	Excluded	63	5 / 7	0.971	N/A	N/A	1.000	1.000	1.000	5 / 7	87	N/A	N/A	100	99	99
		Included	69	6	0.808	0.867	1.000	1.000	1.000	1.000	6	55	63	100	100	100	100
	Reduced	Excluded	63	1 / 2 / 3	0.675*	N/A	N/A	1.000	1.000	1.000	4 / 6	28	N/A	N/A	100	96	98
		Included	69	3	0.685	0.864*	1.000	1.000	1.000	1.000	3	70	69	100	100	100	100
Dog+ceratomorphs (Data set 3)	All	Excluded	71	1 / 2 / 3	0.598*	N/A	N/A	1.000	1.000	1.000	4 / 6	59	N/A	N/A	100	100	100
		Included	77	**1**	**1.000***	**1.000***	1.000	1.000	1.000	1.000	1	94*	**96***	100	100	100	100
	Reduced	Excluded	71	**1 / 2 / 3**	**0.999***	N/A	N/A	1.000	1.000	1.000	1 / 2 / 3	**97***	N/A	N/A	100	100	100
		Included	77	**1**	**1.000***	**1.000***	1.000	1.000	1.000	1.000	1	**99***	**100***	100	100	100	100

Topology numbers and node letters refer to those outlined in Appendix 2-figure 3. Bayesian posterior probability support of >0.99 and ML bootstrap support of >95% are in bold for nodes A and B. *support for nodes that are consistent with topology 1 in Appendix 2-figure 3. NCs: non-caballines.

1287

bioRxiv preprint doi: https://doi.org/10.1101/154963; this version posted June 24, 2017. The copyright holder for this preprint (which was not certified by peer review) is the author/funder. All rights reserved. No reuse allowed without permission.

Supplementary table 2. The *a posteriori* phylogenetic placement likelihood for eight ceratomorph (rhino and tapir) outgroups using a ML evolutionary placement algorithm, whilst varying the partition set used (all or reduced), and either including or excluding *Hippidion* sequences.

***Hippidion*?**	**Outgroup**	**Partitions**	**All**					**Reduced**				
		Topology	**1**	**2**	**3**	**6**	**7**	**1**	**2**	**3**	**6**	**7**
Included	*Tapirus terrestris* (AJ428947)		0.457	0.317	0.205	0.018		0.410	0.391	0.199		
Included	*Tapirus indicus* (NC023838)		0.276	0.105	0.225	0.389		0.536	0.298	0.166		
Included	*Coelodonta antiquitatis* (NC012681)		**0.998**					0.411	0.554	0.035		
Included	*Dicerorhinus sumatrensis* (NC012684)		**0.981**		0.009			**0.983**	0.015			
Included	*Rhinoceros unicornis* (NC001779)		**0.998**					**0.998**				
Included	*Rhinoceros sondaicus* (NC012683)		**0.989**	0.006				0.895	0.102			
Included	*Ceratotherium simum* (NC001808)		0.448	0.499	0.052			0.296	0.704			
Included	*Diceros bicornis* (NC012682)		0.918	0.065	0.018			**0.996**				
		Topology	**1 / 2 / 3**			**4 / 6**	**5 / 7**	**1 / 2 / 3**			**4 / 6**	**5 / 7**
Excluded	*Tapirus terrestris* (AJ428947)		0.550			0.312	0.138	**0.987**				0.012
Excluded	*Tapirus indicus* (NC023838)		0.050			0.908	0.041	**0.995**				
Excluded	*Coelodonta antiquitatis* (NC012681)		0.248			0.451	0.301	**1.000**				
Excluded	*Dicerorhinus sumatrensis* (NC012684)		0.155			0.553	0.291	**1.000**				
Excluded	*Rhinoceros unicornis* (NC001779)		0.530			0.334	0.136	**1.000**				
Excluded	*Rhinoceros sondaicus* (NC012683)		0.733			0.196	0.071	**1.000**				
Excluded	*Ceratotherium simum* (NC001808)		0.949			0.018	0.033	**1.000**				
Excluded	*Diceros bicornis* (NC012682)		0.851			0.073	0.075	**1.000**				

The best supported placement for each analysis has been given a gray background, and likelihoods >0.95 are in bold. Topology numbers refer to those outlined in Appendix 2-figure 3. Genbank accession numbers are given in parentheses after outgroup names.

Supplementary table 3. Bayesian time tree analysis results, with support and estimated divergence times for major nodes, and the tMRCAs for *Haringtonhippus*, *E. asinus*, and *E. quagga* summarized.

E. ovodovi?	Partition	Root prior	*Hippidion-Haringtonhippus/Equus*		*Haringtonhippus-Equus*			*Equus*			*Haringtonhippus*			*E. asinus*			*E. quagga*		
			Node height		Posterior	Node height		Posterior	Node height		Posterior	Node height		Posterior	Node height		Posterior	Node height		
			Median	95% HPD		Median	95% HPD		Median	95% HPD		Median	95% HPD		Median	95% HPD		Median	95% HPD
Included	All	Constrained	6.19	5.22-7.23	0.999	4.59	4.18-5.06	1.000	4.10	3.81-4.39	1.000	0.264	0.198-0.348	1.000	0.720	0.556-0.916	1.000	0.599	0.449-0.770
		Not constrained	6.20	5.20-7.24	1.000	4.59	4.17-5.04	1.000	4.10	3.81-4.38	1.000	0.263	0.196-0.342	1.000	0.719	0.549-0.906	1.000	0.600	0.446-0.770
	Reduced	Constrained	6.30	5.15-7.50	0.997	4.58	4.11-5.11	0.998	4.08	3.77-4.36	1.000	0.334	0.224-0.463	1.000	0.755	0.544-0.992	1.000	0.605	0.411-0.816
		Not constrained	6.35	5.21-7.60	0.996	4.59	4.09-5.09	0.996	4.08	3.79-4.38	1.000	0.335	0.228-0.465	1.000	0.755	0.550-0.998	1.000	0.605	0.412-0.821
Excluded	All	Constrained	6.21	5.22-7.21	1.000	4.58	4.16-5.04	1.000	4.10	3.81-4.39	1.000	0.269	0.200-0.352	1.000	0.735	0.561-0.924	1.000	0.608	0.459-0.777
		Not constrained	6.29	5.33-7.33	1.000	4.60	4.17-5.05	1.000	4.11	3.81-4.40	1.000	0.273	0.200-0.354	1.000	0.742	0.560-0.921	1.000	0.618	0.463-0.791
	Reduced	Constrained	6.44	5.36-7.63	0.999	4.60	4.12-5.11	0.998	4.08	3.78-4.36	1.000	0.338	0.227-0.466	1.000	0.778	0.570-1.020	1.000	0.609	0.431-0.851
		Not constrained	6.49	5.38-7.66	0.999	4.61	4.13-5.13	0.999	4.09	3.79-4.38	1.000	0.339	0.228-0.467	1.000	0.781	0.574-1.027	1.000	0.614	0.423-0.819
		Range	6.19-6.49	5.15-7.66	0.996-1.000	4.58-4.61	4.09-5.13	0.996-1.000	4.08-4.11	3.77-4.40	1.000	0.263-0.339	0.196-0.467	1.000	0.719-0.781	0.544-1.027	1.000	0.599-0.618	0.411-0.851

All analyses supported topology 1 in Appendix 2-figure 3. HPD: highest posterior density.

bioRxiv preprint doi: https://doi.org/10.1101/154963; this version posted June 24, 2017. The copyright holder for this preprint (which was not certified by peer review) is the author/funder. All rights reserved. No reuse allowed without permission.

Supplementary table 4. The *a posteriori* phylogenetic placement likelihood for 12 published equid mitochondrial sequences using the ML evolutionary placement algorithm, whilst varying the partition set used (all or reduced), and either including or excluding *Hippidion* sequences.

		Partitions	**All**				**Reduced**	
***Hippidion*?**	**Published sample**	**Placement**	**Sister to *E. ovodovi***	**Sister to *Hippidion***	**Within NWSL**	**Sister to NWSL**	**Within NWSL**	**Sister to NWSL**
Included	*E. ovodovi* (ACAD2305)		1.000				N/A	N/A
Included	*E. ovodovi* (ACAD2302)		1.000				N/A	N/A
Included	*E. ovodovi* (ACAD2303)		1.000				N/A	N/A
Included	*H. devillei* (ACAD3615)			1.000			N/A	N/A
Included	*H. devillei* (ACAD3625)			1.000			N/A	N/A
Included	*H. devillei* (ACAD3627)			1.000			N/A	N/A
Included	*H. devillei* (ACAD3628)			0.999			N/A	N/A
Included	*H. devillei* (ACAD3629)			0.999			N/A	N/A
Included	NWSL equid (JW125)				0.996		N/A	N/A
Included	NWSL equid (JW126)				0.999		N/A	N/A
Included	NWSL equid (JW328; JX312726)				1.000		0.996	
Included	NWSL equid (MS272; JX312727)					1.000		1.000
Excluded	*E. ovodovi* (ACAD2305)		1.000				N/A	N/A
Excluded	*E. ovodovi* (ACAD2302)		1.000				N/A	N/A
Excluded	*E. ovodovi* (ACAD2303)		1.000				N/A	N/A
Excluded	NWSL equid (JW125)				0.996		N/A	N/A
Excluded	NWSL equid (JW126)				0.999		N/A	N/A
Excluded	NWSL equid (JW328; JX312726)				1.000		0.995	
Excluded	NWSL equid (MS272; JX312727)					1.000		1.000

For mitochondrial genome sequences, sample names and Genbank accession numbers are given in parentheses after the species names. For short mitochondrial DNA fragments, sample names are given in parentheses after the species names.

Supplementary table 5. Summary of nuclear genome data from all 17 NWSL equids pooled together and analyzed using approach four.

Genome coordinates	Fragment length bin (bp)	Count of all sites	Private transversion frequency											
			Absolute			Relative			Combined relative frequencies			Ratio between relative frequencies		
			NWSL	Donkey	Horse	NWSL	Donkey	Horse	NWSL+ Donkey	NWSL+ Horse	Donkey+ Horse	NWSL: Donkey	NWSL: Horse	Donkey: Horse
Horse-based	30-39	49318650	64465	83016	53488	1.307E-03	1.683E-03	1.085E-03	2.990E-03	2.392E-03	2.768E-03	0.777	1.205	1.552
	40-49	59781463	100232	100055	73823	1.677E-03	1.674E-03	1.235E-03	3.350E-03	2.912E-03	2.909E-03	1.002	1.358	1.355
	50-59	57405192	107455	96797	75746	1.872E-03	1.686E-03	1.319E-03	3.558E-03	3.191E-03	3.006E-03	1.110	1.419	1.278
	60-69	49392344	97377	82944	68033	1.971E-03	1.679E-03	1.377E-03	3.651E-03	3.349E-03	3.057E-03	1.174	1.431	1.219
	70-79	41109339	84198	68807	58380	2.048E-03	1.674E-03	1.420E-03	3.722E-03	3.468E-03	3.094E-03	1.224	1.442	1.179
	80-89	28683294	65569	47845	44893	2.286E-03	1.668E-03	1.565E-03	3.954E-03	3.851E-03	3.233E-03	1.370	1.461	1.066
	90-99	17754307	43342	29760	29359	2.441E-03	1.676E-03	1.654E-03	4.117E-03	4.095E-03	3.330E-03	1.456	1.476	1.014
	100-109	10556561	26655	17725	17424	2.525E-03	1.679E-03	1.651E-03	4.204E-03	4.176E-03	3.330E-03	1.504	1.530	1.017
	110-119	6384882	16336	10713	10562	2.559E-03	1.678E-03	1.654E-03	4.236E-03	4.213E-03	3.332E-03	1.525	1.547	1.014
	120-129	3664296	9435	6159	6052	2.575E-03	1.681E-03	1.652E-03	4.256E-03	4.226E-03	3.332E-03	1.532	1.559	1.018
	Total/Mean:	38360046	95768	64357	63397	2.525E-03	1.678E-03	1.652E-03	4.203E-03	4.177E-03	3.331E-03	1.504	**1.528**	1.016
Donkey-based	30-39	28276643	38149	30750	47684	1.349E-03	1.087E-03	1.686E-03	2.437E-03	3.035E-03	2.774E-03	1.241	0.800	0.645
	40-49	34035949	56874	41946	57300	1.671E-03	1.232E-03	1.684E-03	2.903E-03	3.355E-03	2.916E-03	1.356	0.993	0.732
	50-59	32495044	60172	43517	54413	1.852E-03	1.339E-03	1.675E-03	3.191E-03	3.526E-03	3.014E-03	1.383	1.106	0.800
	60-69	27941039	54058	38665	46445	1.935E-03	1.384E-03	1.662E-03	3.319E-03	3.597E-03	3.046E-03	1.398	1.164	0.832
	70-79	23282014	46578	33146	38794	2.001E-03	1.424E-03	1.666E-03	3.424E-03	3.667E-03	3.090E-03	1.405	1.201	0.854
	80-89	16178161	36031	25345	27071	2.227E-03	1.567E-03	1.673E-03	3.794E-03	3.900E-03	3.240E-03	1.422	1.331	0.936
	90-99	9992386	23517	16457	16802	2.353E-03	1.647E-03	1.681E-03	4.000E-03	4.035E-03	3.328E-03	1.429	1.400	0.979
	100-109	5915994	14259	9723	10014	2.410E-03	1.644E-03	1.693E-03	4.054E-03	4.103E-03	3.336E-03	1.467	1.424	0.971
	110-119	3576444	8713	5943	5996	2.436E-03	1.662E-03	1.677E-03	4.098E-03	4.113E-03	3.338E-03	1.466	1.453	0.991
	120-129	2058710	5031	3467	3414	2.444E-03	1.684E-03	1.658E-03	4.128E-03	4.102E-03	3.342E-03	1.451	1.474	1.016
	Total/Mean:	21543534	51520	35590	36226	2.411E-03	1.659E-03	1.677E-03	4.070E-03	4.088E-03	3.336E-03	1.453	**1.437**	0.989

Minimum and maximum NWSL:*Equus* ratios between relative frequencies are in bold, and are used for the divergence estimates in Figure 1-Figure supplement 3. Total and mean values are for the four longest bins only (90-99 to 120-129 bp). Mean values equally weight each length bin. bp: base pairs.

bioRxiv preprint doi: https://doi.org/10.1101/154963; this version posted June 24, 2017. The copyright holder for this preprint (which was not certified by peer review) is the author/funder. All rights reserved. No reuse allowed without permission.

Supplementary table 6. Sex determination analysis of 17 NWSL equids.

Sample	Museum accession	Chromosome ratio	Inferred sex
AF037	YG 402.235	0.48	male
JK166	LACM(CIT) 109/150807	0.93	female
JK167	LACM(CIT) 109/149291	0.91	female
JK207	LACM(CIT) 109/156450	0.92	female
JK260	KU 47800	0.95	female
JK276	KU 53678	0.91	female
MS341	YG 303.1085	0.50	male
MS349	YG 130.55	0.48	male
MS439	YG 401.387	0.98	female
PH008	YG 404.205	0.90	female
PH013	YG 130.6	0.87	probable female
PH014	YG 303.371	0.46	male
PH015	YG 404.662	0.44	male
PH021	YG 29.169	0.83	probable female
PH023	YG 160.8	0.91	female
PH036	YG 76.2	0.81	probable female
PH047	YG 404.663	0.88	probable female

Chromosome ratio is the relative mapping frequency ratio between all autosomes and the X-chromosome. Males are inferred if the ratio is 0.45-0.55 and females if the ratio is 0.9-1.1.

bioRxiv preprint doi: https://doi.org/10.1101/154963; this version posted June 24, 2017. The copyright holder for this preprint (which was not certified by peer review) is the author/funder. All rights reserved. No reuse allowed without permission.

Supplementary table 7. Summary of the number and type of synapomorphic bases for each of the three examined equid genera.

Substitution	***Hippidion***	***Haringtonhippus***	***Equus***
Transition	338	147	66
Transversion	43	22	4
Insertion	2	4	0
Deletion	3	0	0
Total*	391	178	75

A full list of these substitutions, and their position relative to the *E. caballus* reference mitochondrial genome (NC_001640), can be found in Supplementary file 5. *total includes a further five synapomorphic sites that have unique states in each genus.

Supplementary table 8. Selected models of molecular evolution for partitions of the first five mtDNA genome alignment data sets.

Data set	Coding1		Coding2		Coding3		rRNAs		tRNAs		CR		Total length	
	Length	Model	Length	Model	Length	Model	Length	Model	Length	Model	Length	Model	All	Reduced
1. White rhino out	3803	GTR+I+G	3803	HKY+I+G	3803	GTR+I+G	2579	GTR+I+G	1529	HKY+I+G	1066	HKY*+I+G	16583	11714
2. Malayan tapir out	3803	GTR+I+G	3803	HKY+I+G	3803	GTR+I+G	2585	GTR+I+G	1530	HKY+I+G	1065	HKY*+G	16589	11721
3. Dog+ceratomorphs out	3803	GTR+I+G	3803	HKY+I+G	3803	GTR+I+G	2615	GTR+I+G	1540	HKY+I+G	N/A	N/A	15564	11761
4. EPA	3803	GTR+I+G	3803	TrN+I+G	3803	GTR+I+G	2601	GTR+I+G	1534	HKY+I+G	1118	HKY+I+G	16662	11741
5. Equids	3802	TrN+I+G	3802	TrN+I+G	3802	GTR+G	2571	TrN+I+G	1528	HKY+I	971	HKY+G	16476	11703

All lengths are in base pairs. Reduced length excludes the Coding3 and CR partitions. For all RAxML analyses the GTR model was implemented. *The TrN model was selected, but this cannot be implemented in MrBayes and so the HKY model was used. EPA: evolutionary placement algorithm; CR: control region.

bioRxiv preprint doi: https://doi.org/10.1101/154963; this version posted June 24, 2017. The copyright holder for this preprint (which was not certified by peer review) is the author/funder. All rights reserved. No reuse allowed without permission.

Supplementary files

Supplementary file 1. Metadata for all samples used in the mitochondrial genomic analyses.

Supplementary file 2. Statistics from the phylogenetic inference analyses of nuclear genomes using all four approaches. (A) Read mapping statistics. (B) Relative transversion frequencies for approaches 1-3. (C) Relative private transversion frequencies for approach 4.

Supplementary file 3. Data from the sex determination analyses.

Supplementary file 4. Measurement data for (A) equid third metatarsals, which were used in the morphometrics analysis, and (B) other NWSL equid elements.

Supplementary file 5. A compilation of all 634 putative synapomorphic sites in the mitochondrial genome for Hippidion, Haringtonhippus, and Equus (A), with a comparison to the published MS272 mitochondrial genome sequence at the 140 sites with a base state that matches one of the three genera (B).

Supplementary file 6. Rscript used for the morphometric analysis.

Supplementary file 7. TREE files of all mitochondrial trees generated by this study.

Supplementary file 8. NEXUS files of all six mitochondrial genome alignment data sets.

Supplementary file 9. XML files for all BEAST analyses.